

Mid-Cretaceous orogenic gold and molybdenite mineralization in the Independence Creek area, Dawson Range, parts of NTS 115J/13 and 14

Greg G. McKenzie, Murray M. Allan¹, James K. Mortensen, Craig J.R. Hart, Matías Sánchez
Mineral Deposit Research Unit, University of British Columbia, Vancouver, BC

Robert A. Creaser²
Department of Earth & Atmospheric Sciences, University of Alberta, Edmonton, AB

McKenzie, G.G., Allan, M.M., Mortensen, J.K., Hart, C.J.R., Sánchez, M., and Creaser, R.A., 2013. Mid-Cretaceous orogenic gold and molybdenite mineralization in the Independence Creek area, Dawson Range, parts of NTS 115J/13 and 14. In: Yukon Exploration and Geology 2012, K.E. MacFarlane, M.G. Nordling, and P.J. Sack (eds.), Yukon Geological Survey, p. 73-97.

ABSTRACT

The Boulevard gold prospect, located in the Independence Creek area of the Dawson Range, comprises sheeted, auriferous quartz-sulphide-carbonate veins and fault breccia, hosted mainly by mafic schist. The nearby Toni Tiger molybdenum showing is characterized by quartz-molybdenite veins cutting Late Permian meta-aplile and garnet-pyroxene skarn of uncertain age. We present geochronological evidence that gold and molybdenum were deposited at 96-95 Ma, approximately 3 m.y. after intrusion of the Dawson Range batholith and Coffee Creek granite. Fluid inclusions from mineralized quartz veins suggests that gold at Boulevard and molybdenite at Toni Tiger were formed from similar H₂O-CO₂-NaCl type fluids between 279 and 310°C and >1 kbar. We conclude that both are part of the same mineralizing system, and that structurally-hosted gold at the nearby Coffee deposit and in the Moosehorn Range of western Yukon may be broadly related, post-arc orogenic systems developed during exhumation of the Dawson Range in mid-Cretaceous time.

¹ mallan@eos.ubc.ca

INTRODUCTION

The Independence Creek area is a broad upland plateau within the Dawson Range of west-central Yukon, and is incised by stream systems draining north into the Yukon River. The area is located approximately 140 km south of Dawson, 40 km south of the Golden Saddle gold deposit (Kinross Gold Corp.), which contains 1.4 Moz of gold (Underworld Resources Inc., January 19, 2010 press release), and approximately 10 km southwest of the Coffee gold deposit, which contains 3.2 Moz of gold (Kaminak Gold Corp., December 13, 2012 press release) (Fig. 1).

Gold mineralization of the Boulevard zone was first identified by Rimfire Minerals Corp. in 2007 in the headwaters of the Independence Creek drainage. It is a northwest-trending, 450 m by 1.2 km, gold-arsenic-

antimony soil geochemical anomaly with sporadic tellurium and bismuth. Exploration at Boulevard was pursued further by Rimfire in 2008, Silver Quest Resources Ltd. from 2009 to 2011, and Independence Gold Corp. in 2012. Exploration methods at Boulevard have included stream sediment geochemistry, soil geochemistry, trenching, mapping, prospecting, induced polarization and magnetometry surveys, airborne aeromagnetic and radiometric surveys, and diamond drilling.

The Toni Tiger molybdenum showing (Yukon MINFILE 115J 052) is located approximately 2 km east of the Boulevard trend (Fig. 2). Mineralization was discovered by regional silt survey in 1969 by Archer, Cathro and Associates, and the anomaly was attributed to disseminated molybdenite in skarn with associated

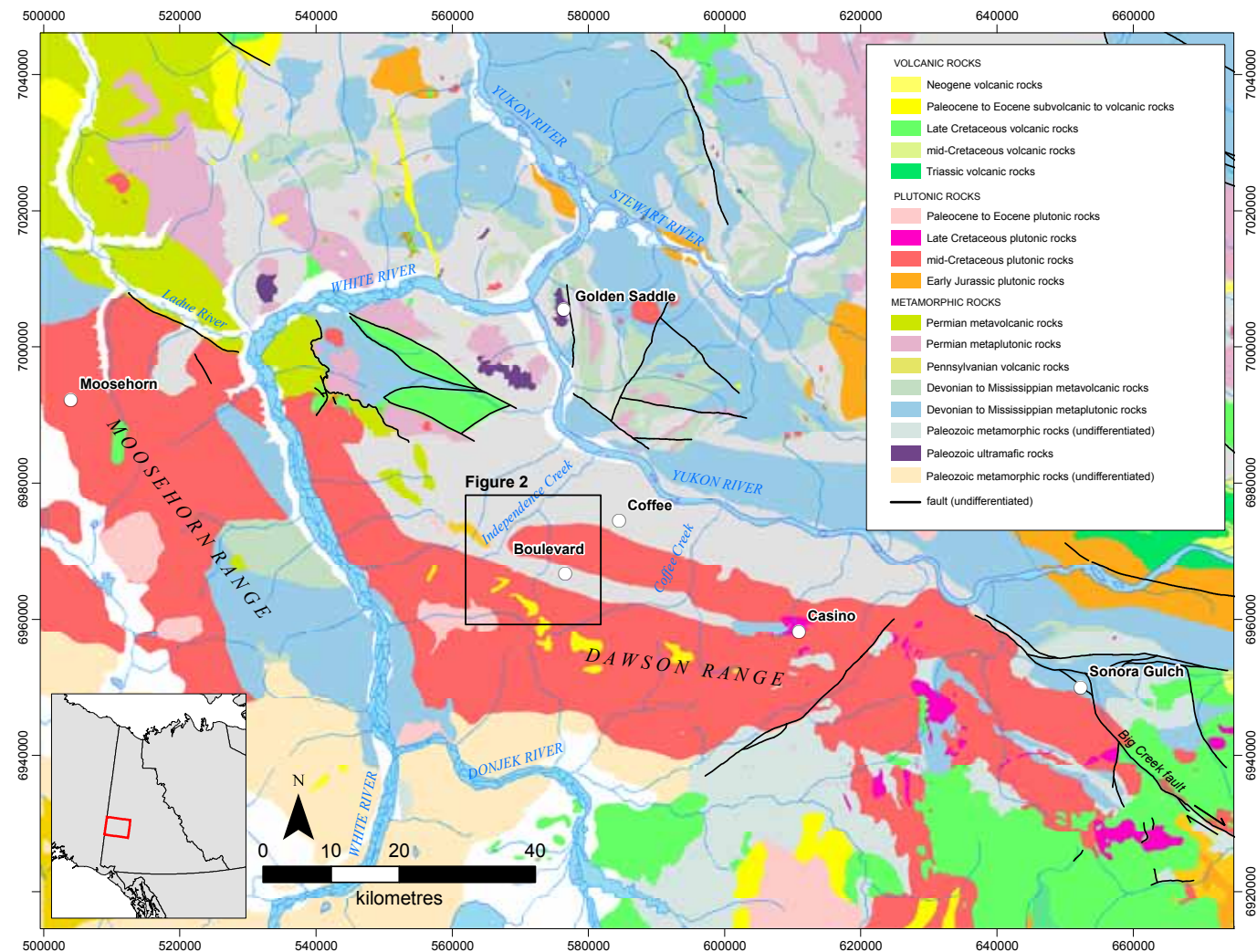


Figure 1. Geological map of the Dawson Range (in greater Yukon Plateau), showing significant mineral deposits and prospects (geology modified from Gordey and Ryan (2005) and Gordey and Makepeace (2003)). The Independence Creek study area is indicated by the black box. Datum: NAD83; Projection: UTM zone 7N.

chalcopyrite, arsenopyrite, scheelite, and pyrite (Craig, 1970). Trenching at the prospect exposed quartz-molybdenite veins, and Craig (1970) inferred that

molybdenite was associated with, and restricted to, the skarn alteration.

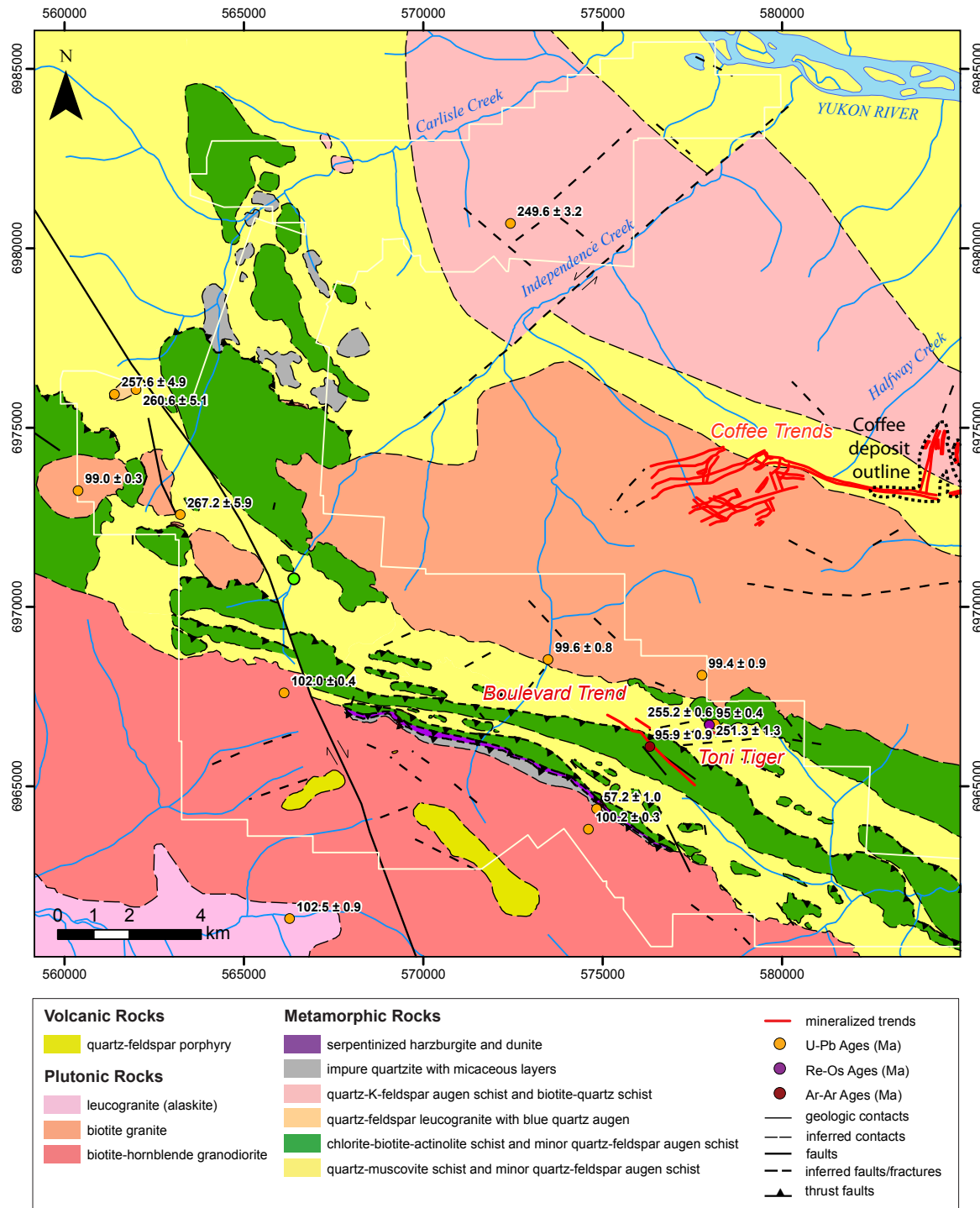


Figure 2. Geologic map of the Independence Creek area, showing geochronological data and mineralized trends in the Boulevard and Coffee prospects (Datum: NAD83; Projection: zone 7N). Additional sources of information include: Tempelman-Kluit, 1974; Jilson, 2000; Gordey and Ryan, 2005; Chartier et al., 2013; J. Ryan, pers. comm., 2012. The white line defines Silver Quest property limits as of June 2011.

The Boulevard and Toni Tiger prospects present an opportunity to investigate the age and geological characteristics of two proximal mineralized systems that have contrasting metal associations (Au-As-Sb and Mo-Cu-W, respectively) and uncertain metallogenesis. The geologic relationships presented below are based on mapping, interpretations of airborne magnetic and radiometric data, and detailed observations of diamond drill core. We present U-Pb zircon ages both for metamorphic rocks (including those hosting molybdenite mineralization), and for samples of the Dawson Range batholith, Coffee Creek plutonic suite, and local subvolcanic units. Petrographic observations and reconnaissance-level fluid inclusion data from mineralized veins are also included. Finally, we present $^{40}\text{Ar}/^{39}\text{Ar}$ muscovite ages for gold-bearing veins at Boulevard and Re-Os molybdenite ages for Toni Tiger, both of which are interpreted to date mineralization directly.

FIELD RELATIONSHIPS

GEOLOGY

The Independence Creek area is underlain by a 3 km-wide, west-northwest-trending belt of predominantly schistose and gneissic rocks (Figs. 1, 2 and 3). This rock package includes the following map units (Fig. 2): (a) serpentinized harzburgite and dunite; (b) variably pyritic chlorite-biotite-actinolite schist, containing minor quartz-feldspar augen schist; (c) quartz-muscovite schist, containing minor calcareous schist; (d) impure quartzite with micaceous layers; (e) foliated quartz-feldspar-muscovite leucogranite and quartz-feldspar augen schist with distinctive blue quartz augen; and (f) quartz-K-feldspar augen schist and minor biotite-quartz schist. Peak metamorphic grade is inferred to be middle greenschist facies on the basis of biotite-chlorite-actinolite assemblages in mafic schists. Lithological heterogeneities are common on the scale of metres to hundreds of metres, due to a combination of original stratigraphic and intrusive contact relationships, and repetition by tight to isoclinal folding and faulting. Ultramafic rocks are exposed as small lenticular bodies near the south margin of the metamorphic package (Figs. 2 and 3f), and are inferred to delineate a major crustal-scale fault (Templeman-Kluit, 1974; Gordey and Makepeace, 2003; Zagorevski *et al.*, 2012).

The metamorphic package is intruded to the south by medium to coarse-grained biotite-hornblende granodiorite of the Dawson Range batholith, a phase of

the mid-Cretaceous Whitehorse plutonic suite (Figs. 1, 2, and 3a). The rock is massive to lineated with locally aligned hornblende and stretched quartz. To the north, metamorphic rocks are intruded by the Coffee Creek phase of the Whitehorse plutonic suite (Templeman-Kluit, 1974), which is composed of medium to coarse-grained biotite granite with volumetrically minor aplitic and pegmatitic phases (Figs. 1, 2, and 3b). A garnet-bearing, quartz-phyric porphyry phase is recognized at the western tip of the Coffee Creek granite. No crosscutting relationships are observed between plutonic rocks and gold mineralization at Boulevard or molybdenite-bearing veins at Toni Tiger.

Locally, subcrop of porphyritic rhyodacite and basalt are observed near the northern margin of the Dawson Range batholith (unit too small to represent on Fig. 2). This unit has been mapped and interpreted as a hypabyssal intrusion (J. Ryan, pers. comm., 2012).

STRUCTURES

The principal fabric within metamorphic rock units in the study area strikes 280-290°N and is steeply dipping between ~70 and 90°. West of the Coffee Creek granite, the strike of the regional metamorphic fabric rotates to 315°N (Fig. 2). This structural pattern in the metamorphic rocks mirrors a major change in the regional strike of the Dawson Range batholith approximately 20 km west of the study area (Fig. 1).

The main metamorphic fabric has strongly transposed any original depositional features within the metamorphic rock units. The development of this fabric is likely due to D₁ and D₂ collisional deformation accompanying peak metamorphism of Yukon-Tanana terrane rocks in Late Permian time (Berman *et al.*, 2007; MacKenzie *et al.*, 2008a; Beranek and Mortensen, 2011). Isoclinal, rootless fold hinges and boudinaged quartz veins are interpreted to represent D₂ phase folds that overprint the earlier S₁ fabric.

A third deformation event (D₃) can be recognized as locally developed crenulations (S₃) and tight disharmonic folding of the pre-existing metamorphic fabric, and is best developed within micaceous lithologies. These folds have axial traces that are subparallel to the regional west-northwest map trend of the metamorphic rock package and axial planes that are subvertical. Ultramafic bodies along the northern margin of the Dawson Range define a lineament that extends eastward toward the Casino Cu-Mo-Au porphyry deposit and the Sonora Gulch porphyry prospect (Fig. 1), and are interpreted to define a crustal-

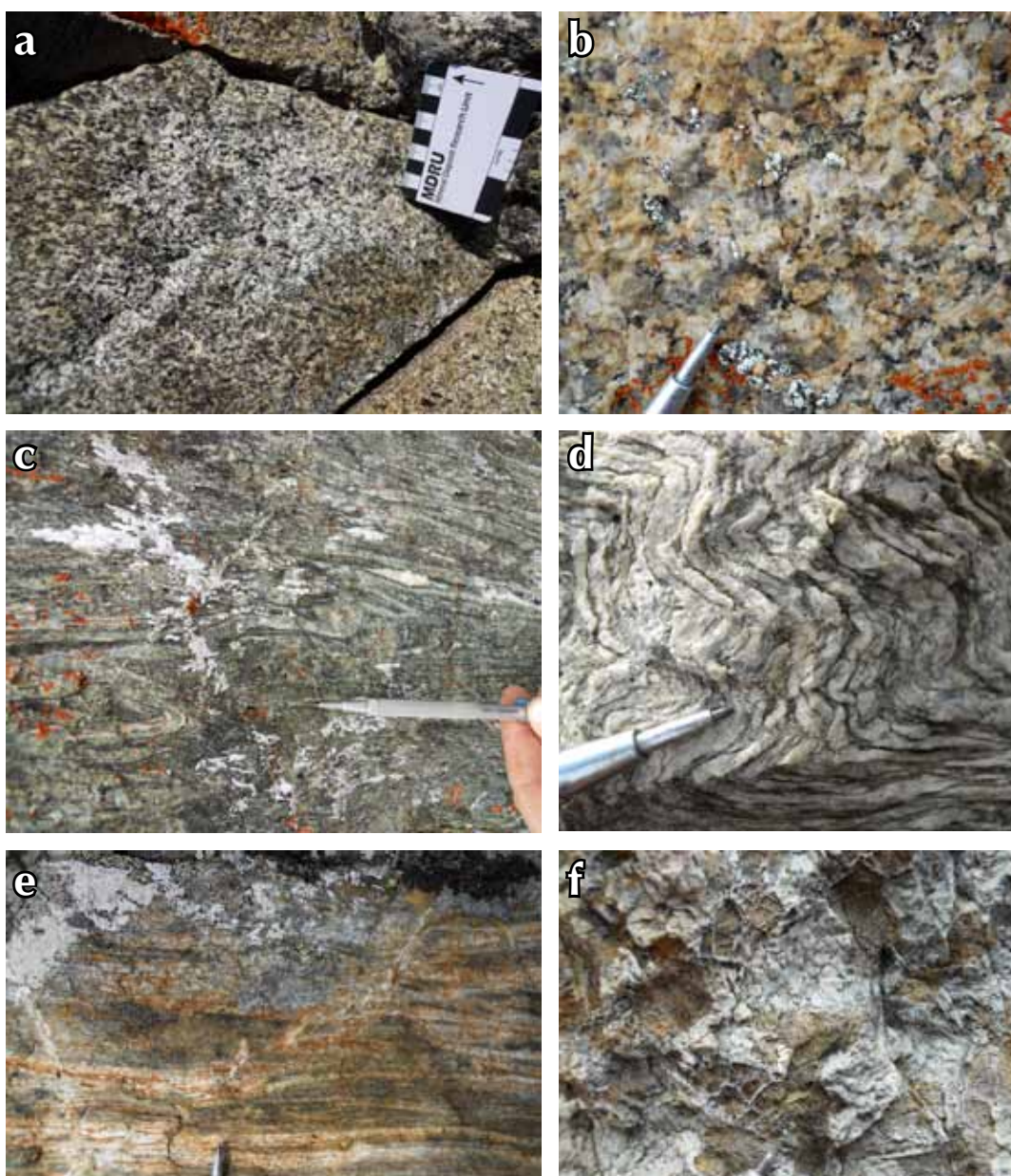


Figure 3. Typical rock types in the Independence Creek area: (a) biotite hornblende granodiorite of the Dawson Range batholith; (b) biotite granite of the Coffee Creek granite; (c) strongly deformed chloritic schist (typical host rock to gold mineralization); (d) folded metagranite; (e) banded diopside-garnet skarn and biotite schist (typical host rock at the Toni Tiger molybdenum showing); and (f) serpentinitized harzburgite.

scale fault that was partially intruded by the Dawson Range batholith (Zagorevski et al., 2012). The origin of this structure is uncertain, but it was likely active in the Early Jurassic, when regional scale thrust faulting imbricated slivers of Slide Mountain oceanic crust within the Yukon-Tanana terrane (MacKenzie et al., 2008a,b; MacKenzie and Craw, 2012).

Locally-developed stretching lineations within the Dawson Range batholith are subhorizontal and parallel to the regional west-northwest strike of metamorphic rocks to the north. The Coffee Creek granite is almost entirely massive, suggesting that either fabrics in the Dawson Range batholith were formed prior to emplacement of the Coffee Creek granite, or that syn to post-magmatic deformation was partitioned more strongly in the Dawson Range batholith.

A fault trending 330°N is obvious in aeromagnetic data, and cuts the metamorphic package and the Dawson Range batholith with 1 km of dextral offset (southwest quadrant of Fig. 2). This fault is the most prominent in a series of northwest to north-northwest-trending structures that truncate the west-northwest-trending magnetic grain of the metamorphic package (Fig. 2). A similar northwest to north-northwest orientation is observed for gold-bearing structures at the Boulevard prospect. The offset of the northern intrusive contact of the Dawson Range batholith by this fault generation indicates that this fault set occurred after emplacement of the Dawson Range batholith in mid-Cretaceous time.

VEINS, ALTERATION, AND MINERALIZATION

Observations on veining, alteration, and mineralization are presented for the Boulevard and Toni Tiger prospects separately, since field relationships do not provide sufficient information about the relative timing of these adjacent systems.

BOULEVARD

Detailed observations of diamond drill core reveal five separate vein generations (Fig. 4), all of which are hosted primarily in biotite-chlorite±actinolite schist. A paragenetic scheme is presented in Figure 5 and petrographic observations are shown in Figure 6.

V₁: The first vein generation (V₁) comprises sugary quartz±pyrite veins, and is found in all metamorphic rock types in the study area (Fig. 4a). V₁ veins are typically ~1 cm wide and contain less than 1% pyrite and trace chalcopyrite as inclusions in pyrite. V₁ veins are conformable with the metamorphic fabric, and commonly occur as boudins and rootless hinges in mesoscopic folds. V₁ veins are early and are interpreted to be

metamorphic segregations formed during Late Permian tectonism.

V₂: V₂ veins are composed of quartz, pyrrhotite±chalcopyrite, are 5 to 30 mm wide, have irregular margins, and no alteration envelopes (Fig. 4b). V₂ veins are generally discordant to the S₁/S₂ fabric, suggesting they post-date peak deformation.

V₃: V₃ veins are composed mainly of quartz and ferroan carbonate with muscovite/illite-pyrite-arsenopyrite

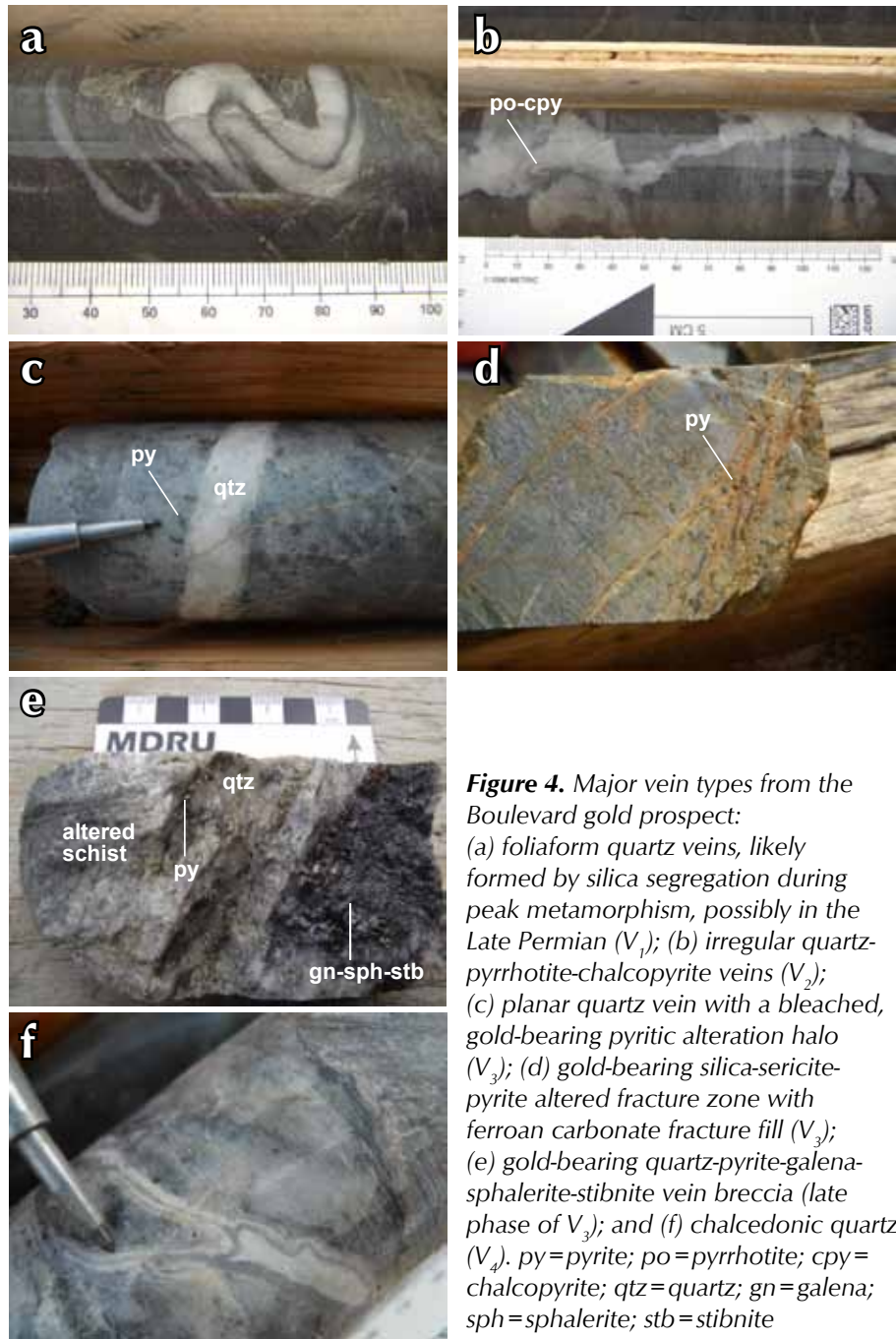


Figure 4. Major vein types from the Boulevard gold prospect: (a) foliaform quartz veins, likely formed by silica segregation during peak metamorphism, possibly in the Late Permian (V₁); (b) irregular quartz-pyrrhotite-chalcopyrite veins (V₂); (c) planar quartz vein with a bleached, gold-bearing pyritic alteration halo (V₃); (d) gold-bearing silica-sericite-pyrite altered fracture zone with ferroan carbonate fracture fill (V₃); (e) gold-bearing quartz-pyrite-galena-sphalerite-stibnite vein breccia (late phase of V₃); and (f) chalcedonic quartz (V₄). py=pyrite; po=pyrrhotite; cpy=chalcopyrite; qtz=quartz; gn=galena; sph=sphalerite; stb=stibnite

	V ₁	V ₂	V ₃	V ₄	V ₅
quartz	—	—	—	—	
ferroan carbonate	—	—	—	—	—
pyrite	—	—	—	—	—
arsenopyrite			—	—	
gold			—	—	
pyrrhotite		—			
chalcocite	—	—			
sphalerite			—		
galena			—		
stibnite			—		
tetrahedrite			—		

Figure 5. Mineral paragenesis for veins present in the Boulevard gold prospect.

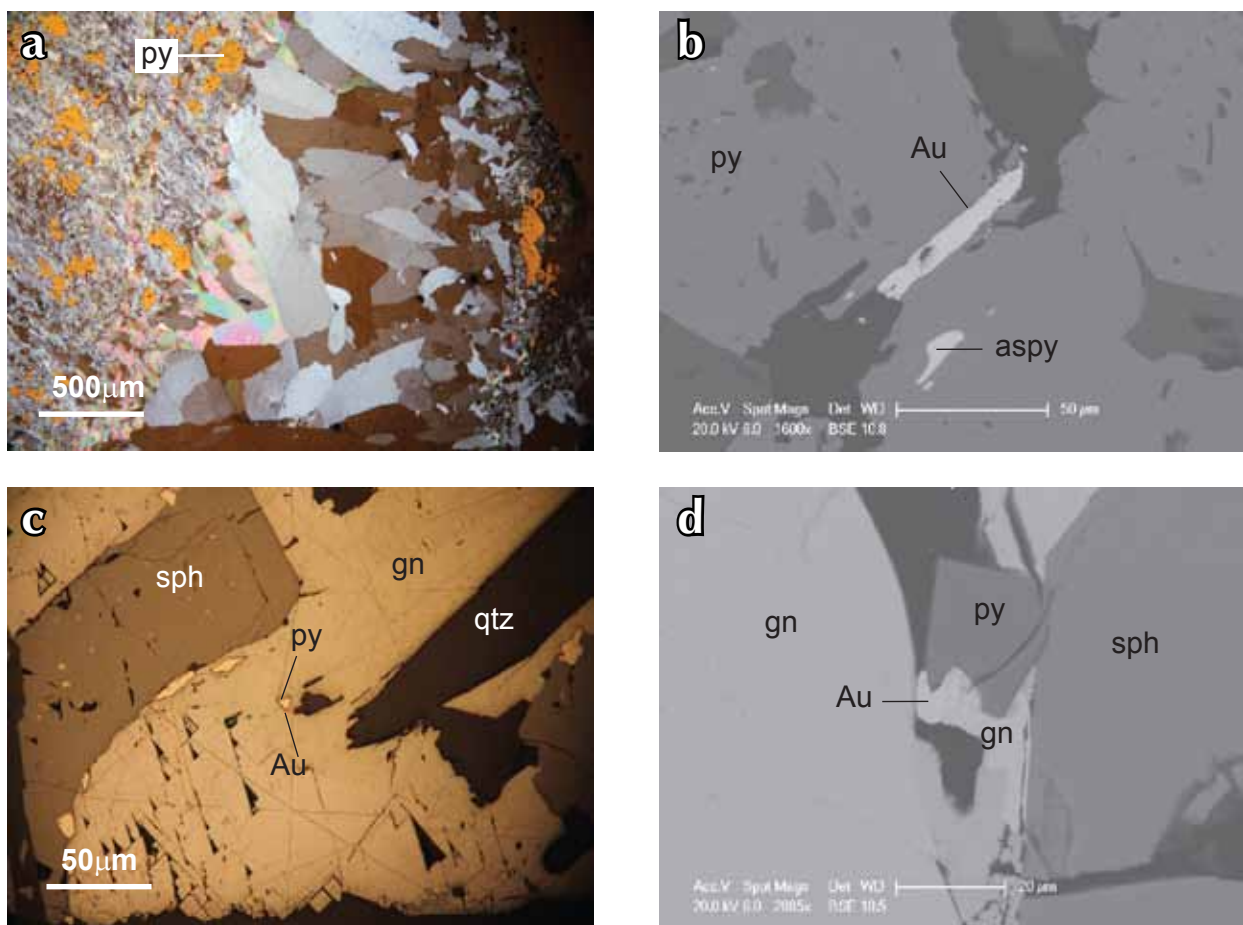


Figure 6. Examples of gold mineralization from the Boulevard area: (a) typical V₃-generation quartz-carbonate vein with a gold-bearing pyrite halo (combined cross-polarized transmitted light and reflected light); (b) backscattered electron microscope image of gold associated with pyrite and arsenopyrite; (c) reflected light photomicrograph of a <5 µm gold grain as an inclusion in galena; (d) backscattered electron microscope image of a 10 µm gold grain associated with galena, sphalerite and pyrite. aspy = arsenopyrite (other mineral abbreviations as in Figure 4).

alteration envelopes (Figs. 4c,d, 6a, and 8a). A paragenetically late phase of sphalerite-galena-pyrite-tetrahedrite±stibnite is observed in some veins, especially where brecciation has also taken place (Fig. 4e). Veins are typically 2 to 20 mm wide, planar, and occur in sheeted sets that cut the S_1/S_2 fabric at a high angle. Approximations of vein orientations (using the local metamorphic fabric as a reference plane in unoriented drill core) yield a predominantly northwest strike and a dip of approximately 30° to the southwest. V_3 vein swarms are spatially related and subparallel to mineralized fault gouge. The faulting is interpreted to post-date V_3 veining since vein fragments have been noted in the fault gouge. Gold has two petrographic associations: (1) inclusions and fracture fillings in pyrite or arsenopyrite in alteration haloes (Fig. 6b); and (2) inclusions in sphalerite-galena-pyrite-tetrahedrite±stibnite (Fig. 6c,d). Gold grains are typically less than 10 μm .

V_4 : A fourth vein generation (V_4) is characterized by thin, colloform banded chalcedonic quartz-carbonate±pyrite±chalcopyrite veins (Fig. 4f). They vary in width from 5 to 60 mm. Carbonate is typically pink and manganiferous. V_4 veins crosscut both the metamorphic fabric and V_3 stage veins.

V_5 : Thin (1-5 mm) ferroan carbonate veinlets (V_5) cut the metamorphic foliation and all pre-existing vein types. This vein generation has no known association with sulphides or gold.

TONI TIGER

The local host rocks include meta-aplite (Fig. 7a,b), biotite-quartz-feldspar schist (Fig. 7c-e), biotite hornfels, and garnet-diopside skarn (Fig. 7f). All rock types are cut by 1 cm to 1 m-wide, milky white quartz±molybdenite veins (Figs. 7c-e and 8c) that occupy subvertical, conjugate fracture sets trending north and northeast. Molybdenite is also observed as wall rock disseminations in vein halos in biotite-quartz-feldspar schist and skarn. Veins have biotite-destructive chlorite-muscovite envelopes where they cut biotite-bearing host rocks (Fig. 7c,f). Idiomorphic garnet of hydrothermal origin is common along the margins of quartz±molybdenite veins cutting the skarn unit.

FLUID INCLUSION PROPERTIES

BOULEVARD

Petrographic observations and a small number of microthermometric analyses were carried out on samples

of quartz-hosted fluid inclusions from gold-stage V_3 veins at Boulevard. A homogenous population of aqueous-carbonic fluid was observed, which, based on clathrate melting and CO₂ homogenization temperatures, contains 15 to 24 mol % CO₂, ~2 to 3 wt % NaCl, and a bulk density of 0.8 to 0.85 g/cm³ (Fig. 8a,b). Homogenization temperatures and equation-of-state modeling, using the approach of Allan et al. (2011), suggest that fluids were trapped between 280 and 310°C or greater, at a pressure of 1100 bar or more. This pressure corresponds to a minimum depth of approximately 4.0 km at lithostatic pressures (assuming a rock density of 2800 kg/m³).

TONI TIGER

A homogenous population of aqueous-carbonic fluid inclusions was observed in vein quartz from Toni Tiger (Fig. 8c). Microthermometric measures of clathrate melting and CO₂ homogenization demonstrate that this fluid contains ~16 mol % CO₂ and ~3 wt % NaCl, with a bulk density of ~0.88 g/cm³ (Fig. 8d). Fluids were trapped at 280°C or more, at a minimum pressure of 1050 bar (>3.8 km at lithostatic pressure, assuming a rock density of 2800 kg/m³). The composition and trapping conditions of fluid inclusions from Toni Tiger veins are therefore indistinguishable from those in V_3 veins at Boulevard.

U-Pb GEOCHRONOLOGY

SAMPLES AND METHODOLOGY

U-Pb dating of zircon was used to determine the crystallization age of various units in the Independence Creek area, including the metamorphic rock package, Dawson Range batholith, Coffee Creek granite, and subvolcanic rocks. The sample suite includes six samples of metaplutonic rocks, including meta-aplite cut by quartz-molybdenite veins at Toni Tiger (I034207); orthogneiss containing minor disseminated molybdenite (I034224); and quartz-feldspar-biotite schist (GM11-9b, MA11-004BV, MA11-005BV, MA11-006BV). The suite also includes three samples of the Dawson Range batholith (I034239, YGR-BV-004, 99M-106-b); three samples of the Coffee Creek phase (YGR-BV-002, 99M-105, 99M-107); and a single sample of quartz-feldspar rhyodacite porphyry (MA11-001BV).

Zircon grains recovered from plutonic and metaplutonic rocks are all relatively coarse grained (up to 200 μm long) and show a similar range of external morphology and internal structure. Zircons are typically clear, euhedral,



Figure 7. Rock types and vein features of the Toni Tiger molybdenum occurrence: (a) weakly foliated meta-aplite from the Toni Tiger occurrence; (b) same meta-aplite as in (a), but interfoliated with biotite schist and affected by a later phase of folding; (c) biotite metagranitoid cut by a quartz-molybdenite vein with a chloritic alteration halo; (d) typical milky quartz vein with molybdenite from the Toni Tiger occurrence; (e) milky quartz vein with molybdenite along its margins (and as wall rock disseminations); and (f) pyroxene-garnet skarn with domains of biotite hornfels. moly = molybdenite.

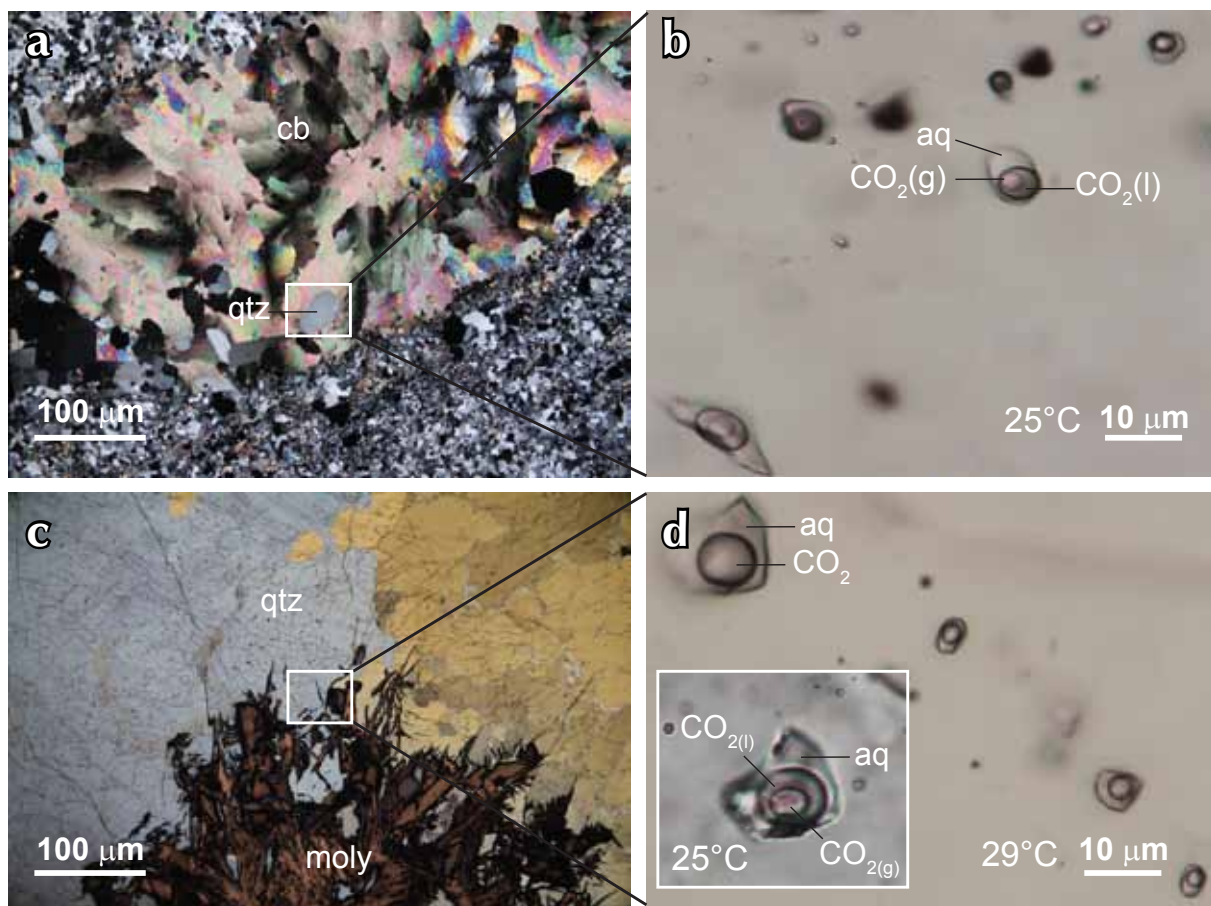


Figure 8. (a) photomicrograph of a V₃-generation quartz-carbonate vein (cross-polarized light) from the Boulevard gold prospect; (b) quartz-hosted fluid inclusions from the vein in (a), containing aqueous liquid (aq), CO₂ liquid, and CO₂ vapour (photograph taken at 25°C); (c) photomicrograph of molybdenite in quartz from the Toni Tiger occurrence (combined cross-polarized transmitted light and reflected light); (d) photomicrograph of fluid inclusions in quartz associated with molybdenite mineralization in (c). Fluid inclusions contain aqueous liquid and a supercritical CO₂ phase (photograph taken just above the homogenization temperature of the carbonic liquid and vapour phase at 29°C). The inset shows both CO₂ phases below the homogenization temperature (~25°C), for the same large fluid inclusion in (d). cb = carbonate; g = gas phase; l = liquid phase; aq = aqueous phase (other abbreviations as in Figures 4 and 7).

and colourless to pale yellow-brown. No obvious internal zoning was observed and morphologies range from stubby octahedral prisms to multi-faceted terminations.

The methodology for laser ablation ICP-MS analysis at the Pacific Centre for Isotopic and Geochemical Research (PCIGR), University of British Columbia, follows that described in Tafti *et al.* (2009) and Beranek and Mortensen (2011). The ²⁰⁶Pb/²³⁸U age is the most precisely determined age for the Phanerozoic zircons in question and is interpreted as the best estimate for the crystallization age of the samples. Assigned ages are based on a weighted average of overlapping, concordant ²⁰⁶Pb/²³⁸U ages of individual analyses for each sample. Errors are quoted at the 2σ level.

RESULTS

Results are presented in conventional U-Pb concordia plots and weighted average ²⁰⁶Pb/²³⁸U age summary plots in Figures 9–12 and are shown with sample locations in Table 1. Full analytical data are presented in Appendix 1.

All meta-igneous samples yielded Late Permian crystallization ages in the range of 250 to 267 Ma (Figs. 9 and 10). The molybdenite-bearing, weakly foliated meta-aplite sample (I034207) from Toni Tiger yields a well-constrained age of 251.3 ± 1.3 Ma (Fig. 9b), which suggests that this unit may be part of a post-D₂ intrusive suite of crustally derived intrusions that includes the Jim Creek pluton of the southern Klondike District (Beranek and

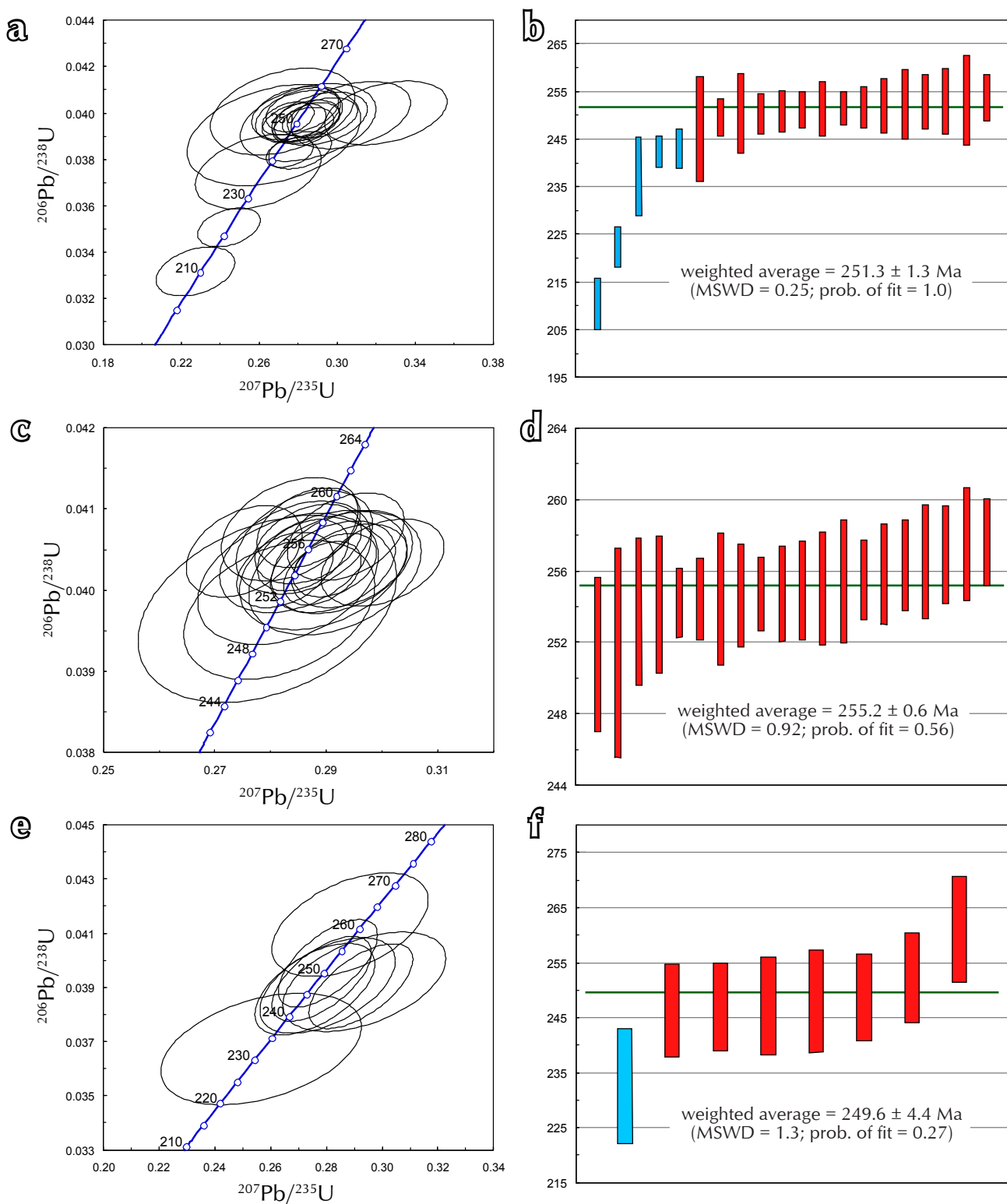


Figure 9. Conventional concordia diagrams and plots of weighted average $^{206}\text{Pb}/^{238}\text{U}$ ages for meta-igneous samples from the study area: (a) and (b) sample I034207 – molybdenite-bearing meta-aplite from Toni Tiger; (c) and (d) sample I034224 - orthogneiss with disseminated molybdenite; (e) and (f) sample GM11-9b – quartz-feldspar-biotite schist. Error ellipses on concordia diagrams and error bars on weighted average age plots are shown at 2s level. Red bars on weighted average age plots were used in the age calculation; blue bars were rejected.

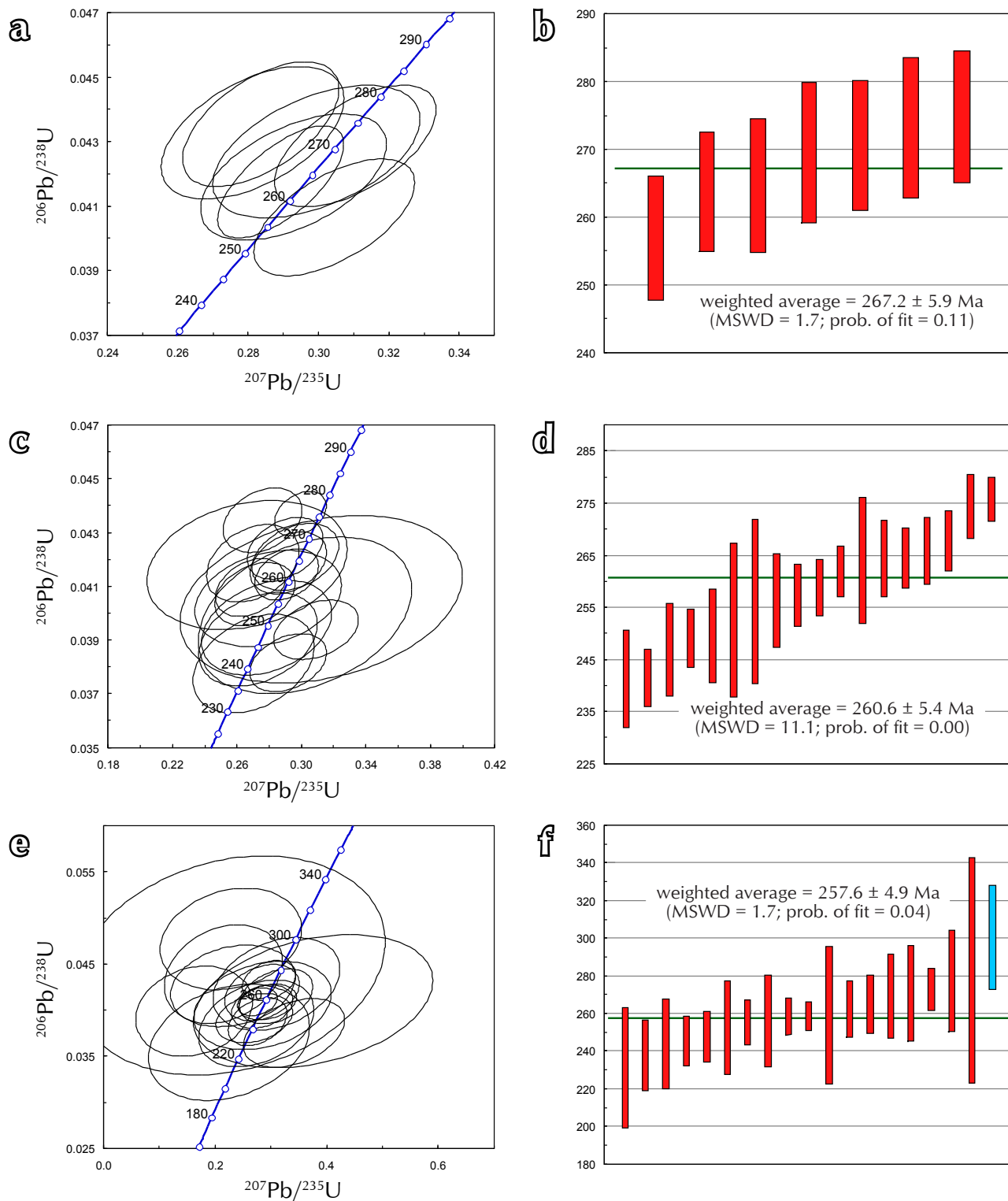


Figure 10. Conventional concordia diagrams and plots of weighted average $^{206}\text{Pb}/^{238}\text{U}$ ages for meta-igneous samples from the study area: (a) and (b) sample MA11-004BV - quartz-feldspar-biotite schist; (c) and (d) sample MA11-00BV - quartz-feldspar-biotite schist; (e) and (f) sample MA11-006BV - quartz-feldspar-biotite schist. Symbols as in Figure 9.

Mortensen, 2011) and the Teacher intrusion in the White Gold area (Mortensen, unpublished data). A sample of quartz-feldspar-biotite schist (GM11-9b) yields a similar age of 249.6 ± 4.4 Ma (Fig. 9f); however, only a small amount of zircon was recovered from this sample and the age is therefore relatively imprecise (based on only seven analyses). All of the other well-foliated meta-igneous rock units yield Late Permian ages ranging from 255 to 267 Ma, which are consistent with ages reported elsewhere for metavolcanic and metaplutonic phases of the Klondike arc assemblage (Mortensen, 1990; Ruks et al., 2006; Beranek and Mortensen, 2011).

Two samples of granodiorite from the Dawson Range batholith give ages of 102.0 ± 0.4 Ma and 100.2 ± 0.3 Ma (Fig. 11b,d). An aplite dyke that cuts Dawson Range granodiorite gives an age of 102.5 ± 0.9 Ma (Fig. 11f). Three biotite granite samples of the Coffee Creek granite give ages ranging from 99 to 100 Ma (Fig. 12b,d,f). The ages are therefore consistent with the Coffee Creek granite being a slightly younger magmatic phase of the Whitehorse plutonic suite than the Dawson Range batholith.

The sample of quartz-feldspar rhyodacite porphyry from subcrop in the study area (sample MA11-001BV) gives an age of 57.2 ± 1.0 Ma (latest Paleocene), which is similar to ages obtained for felsic dykes and plugs throughout the Dawson Range and areas to the north (Mortensen, unpublished data).

$^{40}\text{Ar}/^{39}\text{Ar}$ GEOCHRONOLOGY

SAMPLE AND METHODOLOGY

$^{40}\text{Ar}/^{39}\text{Ar}$ geochronology was used to determine the age of a sample of hydrothermal sericite from a quartz-carbonate-stibnite-gold vein with a strong sericite selvage (sample BV23_70.37m from diamond drill core). The hydrothermal sericite is interpreted to have formed at the same time as gold and stibnite mineralization.

Sericite grains were hand-picked from the sample under a binocular microscope, wrapped in aluminum foil, and stacked in an irradiation capsule with similar-aged samples and neutron flux monitors (Fish Canyon Tuff sanidine (FCS); 28.03 Ma (Renne et al., 1998). The methodology used in this study for $^{40}\text{Ar}/^{39}\text{Ar}$ dating at PCIGR is similar to that described by Mortensen et al. (2010). The Boulevard sericite sample was irradiated from May

4 to 5, 2011 at the McMaster Nuclear Reactor in Hamilton, Ontario, for 45 MWH, with a neutron flux of approximately 6×10^{13} neutrons/cm²/s. Analyses ($n=45$) of 15 neutron flux monitor positions produced errors of <0.5% in the J value. The sample was split into two separate aliquots after irradiation, and the samples were analysed from June through October 2011 at the Noble Gas Laboratory in the PCIGR.

RESULTS

The first aliquot of hydrothermal sericite yielded a plateau age of 95.9 ± 0.9 Ma (MSWD = 0.97, probability = 0.41; plateau based on 74.3% of the ^{39}Ar ; Fig. 13; Table 2). The duplicate analysis did not settle to enough steps to yield a plateau age, but the results are consistent with the age obtained from the first aliquot.

$^{187}\text{Re}/^{187}\text{Os}$ GEOCHRONOLOGY

SAMPLES AND METHODOLOGY

$^{187}\text{Re}/^{187}\text{Os}$ dating methods were utilized to constrain the age of molybdenite mineralization at the Toni Tiger showing. Two samples of molybdenite were dated: (a) a quartz-molybdenite vein crosscutting a meta-aplite (I034208); and (b) a quartz-molybdenite vein crosscutting garnet-actinolite-diopside skarn (I034229). Molybdenite in each sample occurs as coarse-grained rosettes mantled by vein quartz.

Samples were prepared and analysed by R. Creaser at the Radiogenic Isotope Laboratory at the University of Alberta according to the methods described by Selby and Creaser (2004) and Markey et al. (2007).

RESULTS

Analytical results for the two samples are given in Table 3. Sample I034208 yielded a Re-Os age of 95.0 ± 0.4 Ma. Sample I034229 contains high common Os, hence the derived age is sensitive to assumed initial $^{187}\text{Os}/^{188}\text{Os}$ ratio. Assuming an initial $^{187}\text{Os}/^{188}\text{Os}$ value of 0.3, a somewhat younger age of 92.4 ± 0.7 Ma is determined for this sample.

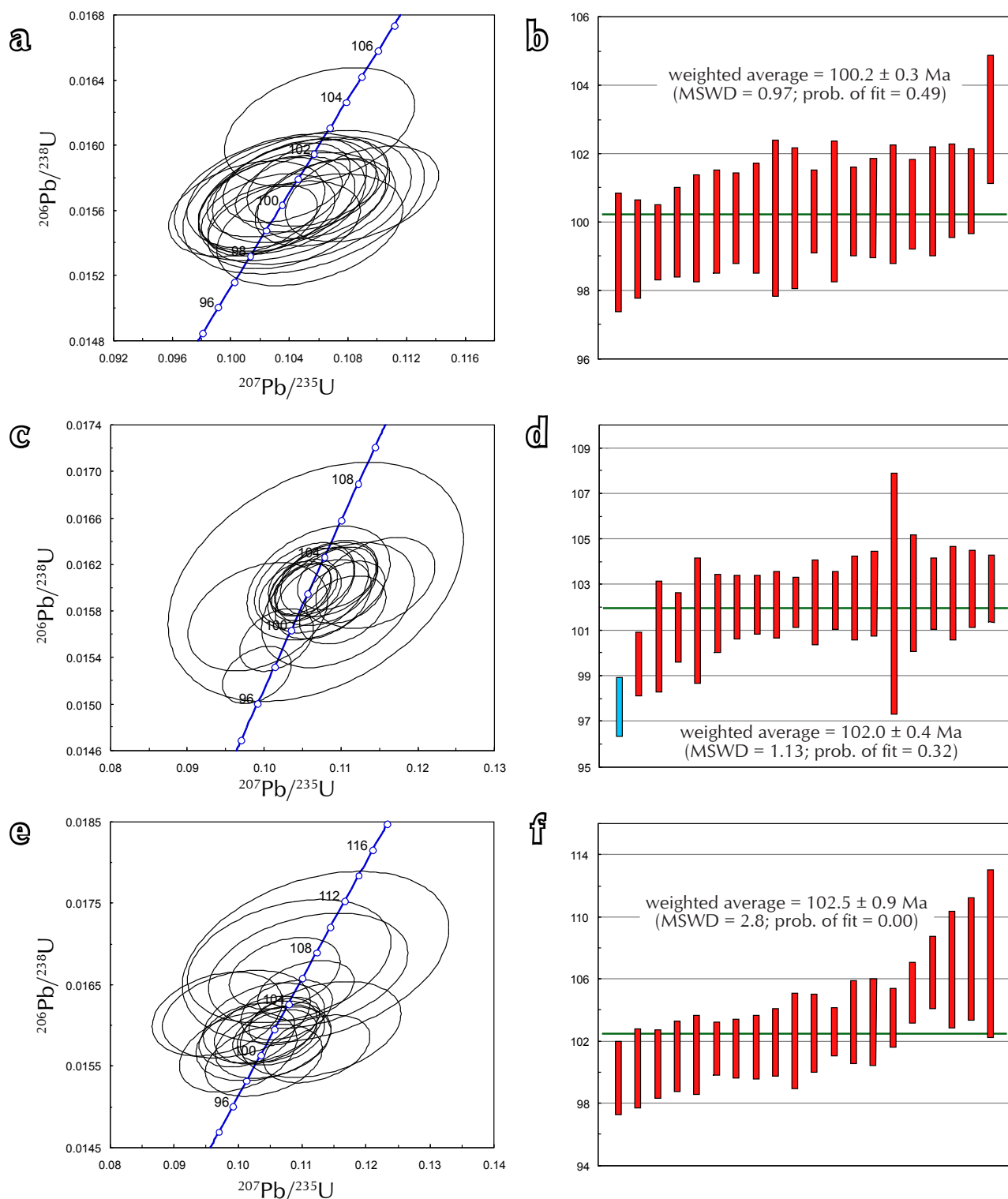


Figure 11. Conventional concordia diagrams and plots of weighted average $^{206}\text{Pb}/^{238}\text{U}$ ages for samples of the Dawson Range batholith in the study area: (a) and (b) sample I034239 - biotite-hornblende granodiorite; (c) and (d) sample YGP-BV-004 - biotite-hornblende granodiorite; (e) and (f) sample 99M-106-b – aplite dyke cutting granodiorite. Symbols as in Figure 9.

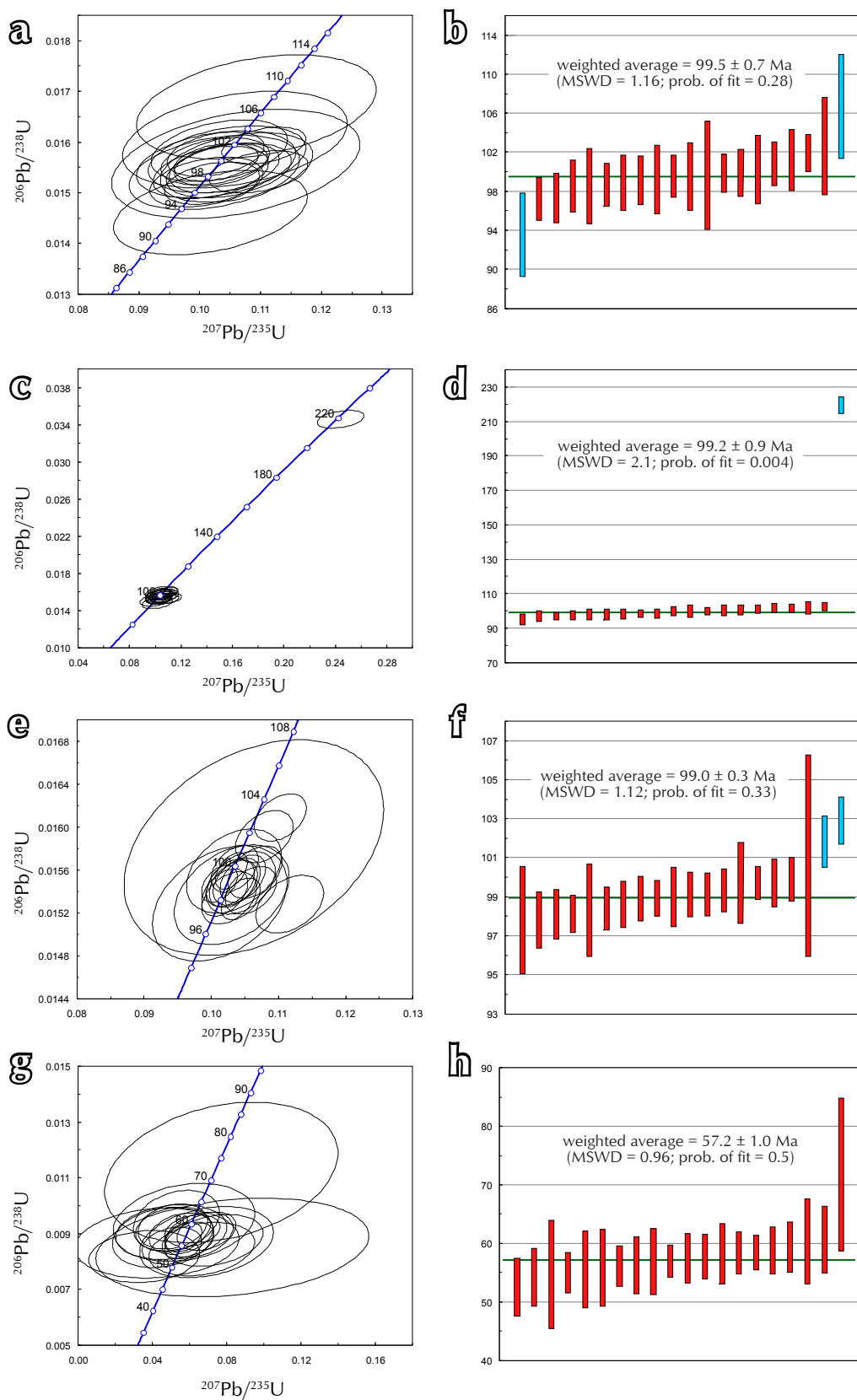


Figure 12. Conventional concordia diagrams and plots of weighted average $^{206}\text{Pb}/^{238}\text{U}$ ages for samples of the Coffee Creek intrusions and a young subvolcanic rock in the study area: (a) and (b) sample YGR-BV-002 – biotite granite; (c) and (d) sample 99M-105 – biotite granite; (e) and (f) sample 99M-107 – biotite granite; (g) and (h) sample MA11-001BV - quartz-feldspar rhyodacite porphyry. Symbols as in Figure 9.

Table 1. $^{206}\text{Pb}/^{238}\text{U}$ zircon ages for Independence Creek samples.

Sample	Rock Description	Unit	Location (NAD83 UTM zone 7N)		Age (Ma)	$\pm 2\sigma$
			Easting	Northing		
METAMORPHIC ROCKS						
I034207	meta-aplite*	Klondike assemblage	577980	6966729	251.3	1.3
I034224	felsic orthogneiss*	Klondike assemblage	578139	6966731	255.2	0.6
GM11-9b	quartz-feldspar-biotite schist	Klondike assemblage	572444	6980691	249.6	4.4
MA11-004BV	quartz-feldspar-biotite schist	Klondike assemblage	563229	6972572	267.2	5.9
MA11-005BV	quartz-feldspar-biotite schist	Klondike assemblage	561996	6976060	260.6	5.4
MA11-006BV	quartz-feldspar-biotite schist	Klondike assemblage	561398	6975930	257.6	4.9
PLUTONIC ROCKS						
I034239	biotite-hornblende granodiorite	Dawson Range batholith	574610	6963807	100.2	0.3
YGR-BV-004	biotite-hornblende granodiorite	Dawson Range batholith	566127	6967606	102.0	0.4
99M-106-b	aplite cutting granodiorite	Dawson Range batholith	566278	6961313	102.5	0.9
YGR-BV-002	biotite granite*	Coffee Creek granite	573497	6968539	99.5	0.7
99M-105	biotite granite	Coffee Creek granite	577775	6968097	99.2	0.9
99M-107	biotite granite	Coffee Creek granite	560386	6973241	99.0	0.3
SUBVOLCANIC ROCKS						
MA11-001BV	quartz-feldspar rhyodacite porphyry	Skukum volcanic suite	574845	6964377	57.2	1.0

*molybdenite observed in heavy mineral separates

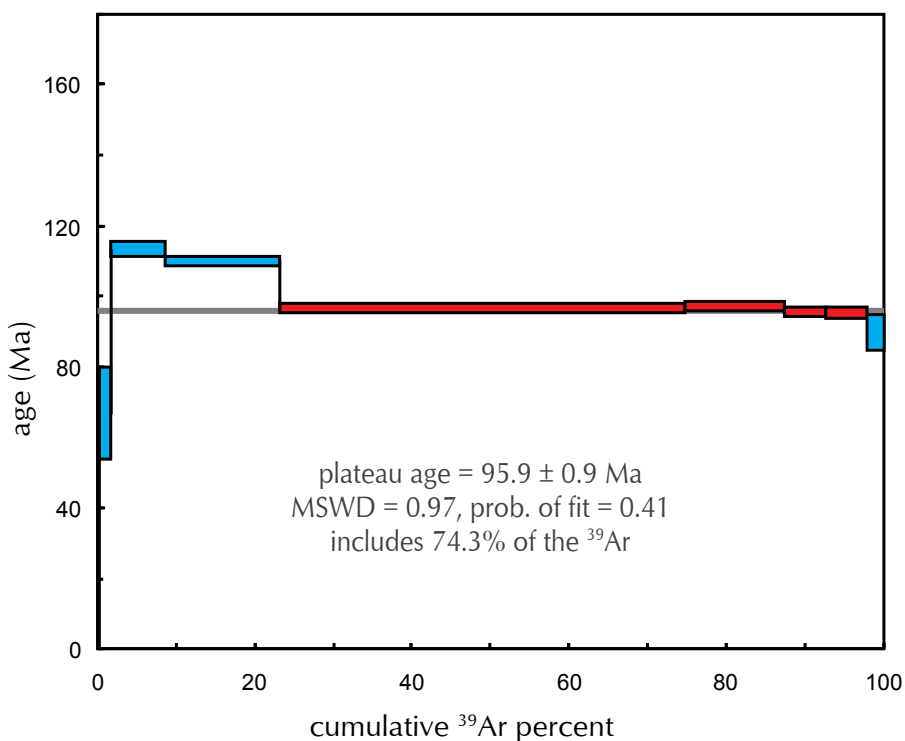


Figure 13. Age spectra for step-heating of sericite sample BV23-70.37m from the Boulevard property. Error boxes and the calculated age are given at the 2σ level. Steps shown in red define the calculated plateau age; steps in blue were rejected.

Table 2. $^{40}\text{Ar}/^{39}\text{Ar}$ data for Boulevard sericite (Sample BV23_70.37m)

Laser power (%)	Isotope Ratios											
	$^{40}\text{Ar}/^{39}\text{Ar}$	1σ	$^{37}\text{Ar}/^{39}\text{Ar}$	1σ	$^{36}\text{Ar}/^{39}\text{Ar}$	1σ	Ca/K	% ^{40}Ar atm	f ^{39}Ar	$^{40}\text{Ar}^*/^{39}\text{ArK}$	Age	2σ
2.20 W	22.38	0.40	0.62	0.09	0.067	0.006	1.13	88.77	0.34	2.515	27.44	± 39.95
2.60 W	24.21	0.22	0.07	0.03	0.061	0.002	0.12	74.58	1.54	6.154	66.43	± 12.64
3.00 W	13.67	0.09	0.47	0.02	0.010	0.000	0.87	22.50	6.68	10.596	112.92	± 2.08
3.50 W	10.72	0.07	0.28	0.01	0.002	0.000	0.52	4.35	14.70	10.259	109.44	± 1.43
4.00 W	9.20	0.06	0.01	0.00	0.001	0.000	0.02	2.27	51.34	8.987	96.21	± 1.17
4.40 W	9.26	0.06	0.01	0.00	0.001	0.000	0.02	2.69	12.50	9.014	96.50	± 1.23
5.00 W	9.70	0.06	0.02	0.01	0.003	0.000	0.04	8.38	5.12	8.891	95.22	± 1.59
6.00 W	10.11	0.06	0.06	0.01	0.004	0.000	0.10	12.15	5.39	8.883	95.13	± 1.61
7.00 W	13.01	0.14	0.02	0.02	0.016	0.001	0.03	35.99	2.39	8.330	89.36	± 5.12
J = 0.0060810 ± 0.0000304	Volume $^{39}\text{ArK} = 0.378$				Integrated Date = 99.34 ± 0.58 Ma							
Plateau age = 95.93 ± 0.89 Ma (2 σ , including J-error of 0.6%)	MSWD = 0.97, probability = 0.41				Includes 74.3% of the ^{39}Ar (steps 5 through 8)							
Inverse isochron (correlation age) results, plateau steps: Model 1 Solution ($\pm 95\%-$ conf.) on 9 points					Age = 98.4 ± 7.6 Ma							
Initial $^{40}\text{Ar}/^{36}\text{Ar} = 350 \pm 170$	MSWD = 75, probability = 0											

Table 3. Re-Os data for Toni Tiger molybdenite samples.

Sample	Re (ppm)	$\pm 2\sigma$	^{187}Re (ppb)	$\pm 2\sigma$	^{187}Os (ppb)	$\pm 2\sigma$	Total common Os (pg)	Model Age (Ma)	$\pm 2\sigma$
I034208	42.96	0.11	27002	71	42.76	0.04	1.6	95.0	0.4
I034208 (duplicate)	43.00	0.11	27029	70	42.76	0.04	1.6	94.9	0.4
I034228	27.62	0.08	17361	53	26.74	0.16	90.8	92.4	0.7

DISCUSSION

U-Pb GEOCHRONOLOGY

The 250 to 267 Ma age range of meta-igneous rocks in the Independence Creek area overlaps with that of the Late Permian Klondike volcanic arc assemblage and intrusive equivalents (Sulphur Creek orthogneiss) elsewhere in western Yukon (Mortensen, 1990; Ruks et al., 2006; Beranek and Mortensen, 2011). We therefore concur with recent mapping by the Geological Survey of Canada which demonstrates that exposures of Klondike arc rocks in the Ladue River area (NTS 115N) continue eastward along the northern margin of the Dawson Range batholith into the Stevenson Ridge map sheet (NTS 115J) (Ryan et al., in prep.).

The mid-Cretaceous crystallization ages determined for the Dawson Range batholith (ca. 100 to 103 Ma) are consistent with current geochronological compilations (Breitsprecher and Mortensen, 2004). The slightly younger 99 to 100 Ma zircon ages for the Coffee Creek granite are consistent with the interpretation of Templeman-Kluit and Wanless (1975) that this unit is a slightly younger intrusive phase of the Whitehorse plutonic suite.

Subvolcanic rocks cutting the Dawson Range batholith were determined to be 57.2 ± 1.0 Ma, and are therefore age-equivalent to the previously mapped Paleocene Skukum volcanic rocks 4 km to the south (Templeman-Kluit, 1974), and volcanic and subvolcanic rocks elsewhere in western Yukon (Breitsprecher and Mortensen, 2004).

TIMING OF MINERALIZATION

The 95.0 ± 0.4 Ma $^{187}\text{Re}/^{187}\text{Os}$ model age for molybdenite at Toni Tiger overlaps within 2σ error with the 95.9 ± 0.9 Ma $^{40}\text{Ar}/^{39}\text{Ar}$ cooling age for hydrothermal sericite at Boulevard. While the latter age could be interpreted as a minimum, there is sufficient geological evidence (e.g., common structural style and fluid inclusion properties) that Boulevard and Toni Tiger are related hydrothermal systems. Therefore, we interpret the $^{187}\text{Re}/^{187}\text{Os}$ and $^{40}\text{Ar}/^{39}\text{Ar}$ methods as recording coeval mineralizing events at ca. 96-95 Ma. Importantly, the mineralization age post-dates crystallization of the Dawson Range batholith and Coffee Creek granite by 3-4 m.y. No younger phase of the Whitehorse plutonic suite has yet been recognized in the Independence Creek area (or anywhere else in western Yukon), nor do the field relationships suggest a magmatic role in mineralization. It is likely that heat and fluid flux related to the emplacement of the Dawson Range batholith and Coffee Creek plutonic suites were responsible for hornfelsing and skarnification in the vicinity of the Toni Tiger showing. However, the geochronologic results of this study suggest that Au-As-Sb-(Pb-Zn-Cu) and Mo mineralization record a distinct and younger event.

The low-salinity, aqueous-carbonic composition of fluids attending mineralization is consistent with orogenic fluids documented worldwide (Groves et al., 2003). The association between gold and pyritic alteration halos to quartz-carbonate veins suggests that wall rock sulphidation is an important gold-precipitating mechanism. Depressurization associated with faulting and brecciation may also play an important role in destabilizing gold-bisulphide complexes (e.g., Wilkinson and Johnston, 1996).

Molybdenite is not commonly reported in orogenic systems; however, the geochronological and fluid inclusion evidence suggests that Toni Tiger is part of the same post-magmatic orogenic system as Boulevard. The association of molybdenite with moderate temperature, moderate pressure, dilute aqueous-carbonic fluids implies that molybdenite transport occurs in nature at $P-T-X$ conditions quite dissimilar to those encountered in high-temperature, low-pressure systems such as porphyry Mo deposits. We speculate that molybdenite may have been remobilized from the felsic metaplutonic host rocks, which locally contain significant background concentrations of molybdenite.

REGIONAL SIGNIFICANCE

This study contributes to the metallogenic framework of the Dawson Range, and may be relevant to other structurally-hosted gold prospects, such as the Coffee gold deposit northeast of the Independence Creek drainage (Kaminak Gold Corp.), and gold in the Moosehorn Range (parts of NTS 115N and 115K; Fig. 1). Mineralization in the Coffee area occurs within a series of structural corridors that cut all rock units, including the mid-Cretaceous Coffee Creek granite (Wainwright et al., 2011). A common, ca. 96-95 Ma metallogenesis for gold mineralization at Boulevard and Coffee is permissible given field relationships, although Coffee is dominated by brittle (shallow?) features, whereas vein swarms at Boulevard more likely represent deeper crustal levels. In the case of the Moosehorn Range, mineralization has been dated by $^{40}\text{Ar}/^{39}\text{Ar}$ methods to 93-92 Ma, which post-dates the main phase of the magmatism by ~8 m.y. (Joyce, 2002). Fluid inclusions associated with the Moosehorn veins also overlap strongly in composition and trapping conditions with those at Boulevard. On the basis of currently available geochronological data and geological relationships, we propose a general model in which exhumation of the Dawson Range shortly after cessation of arc magmatism in mid-Cretaceous time was accompanied by brittle deformation, fluid flow, and mineralization. However, the tectonic and structural setting of the Dawson Range at this time is still not completely understood.

ACKNOWLEDGEMENTS

This study is part of GGM's MSc project, which was a component of the Yukon Gold Project, a collaborative research venture between the Mineral Deposit Research Unit (UBC) and a consortium of industry participants, including Aldrin Resource Corp., Barrick Gold Corp., Full Metal Minerals Corp., Gold Fields Canada Exploration, Northern Freegold Resources Ltd., Kinross Gold Corp., Radius Gold Inc., Silver Quest Resources Ltd., Taku Gold Corp., Teck Resources Ltd., and Underworld Resources Inc. The Natural Science and Engineering Research Council of Canada (NSERC) also provided matching funds for the industry contribution. We are grateful for the logistical, financial, scientific, and editorial contributions of Silver Quest Resources (now Independence Gold Corp.) and Equity Exploration Ltd., and in particular Kendra Johnston, Darcy Baker, Dave Pawliuk, Randy Turner, and Ryan Congdon. Jim Ryan of the Geological Survey of Canada is thanked for his thoughtful review and his contributions to the geological understanding of the Dawson Range.

REFERENCES

- Allan, M.M., Morrison, G.W., and Yardley, B.W.D., 2011. Physicochemical evolution of a porphyry-breccia system: a laser ablation ICP-MS study of fluid inclusions in the Mount Leyshon Au deposit, Queensland, Australia. *Economic Geology*, vol. 106, no. 3, p. 413-436.
- Beranek, L.P. and Mortensen, J.K., 2011. The timing and provenance record of the Late Permian Klondike orogeny in northwestern Canada and arc-continent collision along western North America. *Tectonics*, vol. 30, no. 5, p. TC5017.
- Berman, R.G., Ryan, J.J., Gordey, S.P., and Villeneuve, M., 2007. Permian to Cretaceous polymetamorphic evolution of the Stewart River region, Yukon-Tanana Terrane, Yukon, Canada; P-T evolution linked with *in situ* SHRIMP monazite geochronology. *Journal of Metamorphic Geology*, vol. 25, p. 803-827.
- Breitsprecher, K. and Mortensen, J.K. (comps.), 2004. YukonAge 2004: A database of isotopic age determinations for rock units from Yukon Territory. Yukon Geological Survey, CD-ROM.
- Craig, D.B., 1970. Toni Tiger report: Soil and rock sampling, bulldozer trenching. Yukon mining assessment report number 060249.
- Chartier, D., Couture, J.-F., Sim., R., and Starkey, J., 2013. Mineral resource evaluation, Coffee gold project, Yukon, Canada: Vancouver, Kaminak Gold Corp., 203 p. <http://kaminak.com/projects/sections_and_maps/reports/technical_report/> [accessed February 10, 2013]
- Gordey, S.P. and Makepeace, A.J. (comps.), 2003. Yukon Digital Geology. Geological Survey of Canada, Open File 1749 and Yukon Geological Survey, Open File 2003-9(D).
- Gordey, S.P. and Ryan, J.J., 2005. Geology, Stewart River area (115N, 115O and part of 115J), Yukon Territory. Geological Survey of Canada, Open File 4970, scale 1:250 000.
- Groves, D.I., Goldfarb, R.J., Robert, F., and Hart, C.J.R., 2003. Gold deposits in metamorphic belts: Overview of current understanding, outstanding problems, future research, and exploration significance. *Economic Geology*, vol. 98, p. 1-29.
- Jilson, G., 2000. Geochemical and geological report on the Dan, Man and Indy claims. Yukon mining assessment report number 094174.
- Joyce, N.L., 2002. Geologic setting, nature, and structural evolution of intrusion-hosted Au-bearing quartz veins at the Longline occurrence, Moosehorn Range Area, west-central Yukon Territory. Unpublished MSc Thesis, University of British Columbia, Vancouver, 201 p.
- MacKenzie, D., Craw, D., and Mortensen, J.K., 2008a. Structural controls on orogenic gold mineralisation in the Klondike goldfield, Canada. *Mineralium Deposita*, vol. 43, p. 435-448.
- MacKenzie, D., Craw, D., and Mortensen J.K., 2008b. Thrust slices and associated deformation in the Klondike goldfields, Yukon. In: Yukon Exploration and Geology 2007, D.S. Emond, L.R. Blackburn, R.P. Hill and L.H. Weston (eds.), Yukon Geological Survey, p. 199-213.
- MacKenzie, D. and Craw, D., 2012. Contrasting structural settings of mafic and ultramafic rocks in the Yukon-Tanana terrane. In: Yukon Exploration and Geology 2011, K.E. MacFarlane and P.J. Sack (eds.), Yukon Geological Survey, p. 115-127.
- Markey, R., Stein, H.J., Hannah, J.L., Zimmerman, A., Selby, D. and Creaser, R.A., 2007. Standardizing Re-Os geochronology: A new molybdenite Reference Material (Henderson, USA) and the stoichiometry of Os salts. *Chemical Geology*, vol. 244, p. 74-87.
- Mortensen, J.K., 1990. Geology and U - Pb geochronology of the Klondike District, west - central Yukon Territory. *Canadian Journal of Earth Sciences*, vol. 27, p. 903-914.
- Mortensen, J.K., Craw, D., MacKenzie, D.J., Gabites, J.E., and Ullrich, T., 2010. Age and origin of orogenic gold mineralization in the Otago Schist Belt, South Island, New Zealand: Constraints from lead isotope and $^{40}\text{Ar}/^{39}\text{Ar}$ dating studies. *Economic Geology*, vol. 105, p. 777-793.
- Renne, P.R., Swisher, C.C., Deino, A.L., Karner, D.B., Owens, T.L., and DePaolo, D.J., 1998. Intercalibration of standards, absolute ages and uncertainties in $^{40}\text{Ar}/^{39}\text{Ar}$ dating. *Chemical Geology*, vol. 145, p. 117-152.
- Ruks, T.W., Piercy, S.J., Ryan, J.J., Villeneuve, M.E., and Creaser, R.A., 2006. Mid- to late Paleozoic K-feldspar augen granitoids of the Yukon-Tanana terrane, Yukon, Canada: Implications for crustal growth and tectonic evolution of the northern Cordillera. *Geological Society of America Bulletin*, vol. 118, p. 1212-1231.

- Selby, D. and Creaser, R.A., 2004. Macroscale NTIMS and microscale LA-MC-ICP-MS Re-Os isotopic analysis of molybdenite: Testing spatial restrictions for reliable Re-Os age determinations, and implications for the decoupling of Re and Os within molybdenite. *Geochimica et Cosmochimica Acta*, vol. 68, p. 3897-3908.
- Tafti, R., Mortensen, J.K., Lang, J.R., Rebagliati, M., and Oliver, J.L., 2009. Jurassic U-Pb and Re-Os ages for the newly discovered Xietongmen Cu-Au porphyry district, Tibet, PRC: Implications for metallogenic epochs in the southern Gangdese belt. *Economic Geology*, vol. 104, p. 127-136.
- Templeman-Kluit, D.J., 1974. Reconnaissance geology of Aishihik Lake, Snag and part of the Stewart River map areas, west-central Yukon Territory. Geological Survey of Canada, Paper 73-14, 93 p.
- Tempelman-Kluit, D. and Wanless, R., 1975. Potassium-argon age determinations of metamorphic and plutonic rocks in the Yukon Crystalline Terrane. *Canadian Journal of Earth Sciences*, vol. 12, p. 1895-1909.
- Wainwright, A.J., Simmons, A.T., Finnigan, C.S., Smith, T.R., and Carpenter, R.L., 2011. Geology of new gold discoveries in the Coffee Creek area, White Gold District, west-central Yukon. In: Yukon Exploration and Geology 2010, K.E. MacFarlane, L.H. Weston, and C. Relf (eds.), Yukon Geological Survey, p. 233-247.
- Wilkinson, J.J. and Johnston, J.D., 1996. Pressure fluctuations, phase separation, and gold precipitation during seismic fracture propagation. *Geology*, vol. 24, p. 395-398.
- Yukon MINFILE, 2010. Yukon MINFILE - A database of mineral occurrences. Yukon Geological Survey, <www.geology.gov.yk.ca/databases_gis.html> [accessed October 17, 2012].
- Zagorevski, A., Ryan, J., Roots, C., and Hayward, N., 2012. Ultramafic rock occurrences in the Dawson Range and their implications for the crustal structure of Yukon-Tanana terrane, Yukon (parts of 115I, J and K), Geological Survey of Canada, Open File 7105, 1 sheet. doi:10.4095/290992.

APPENDIX 1: LA-ICP-MS data for U-Pb analysis of zircons

APPENDIX 1 (continued): LA-ICP-MS data for U-Pb analysis of zircons

Fraction	Isotopic Ratios						Isotopic Ages						Background corrected mean counts per second at specified mass											
	$^{207}\text{Pb}/^{235}\text{U}$	% 1 σ	$^{208}\text{Pb}/^{235}\text{U}$	% 1 σ	r_{Ho}	$^{207}\text{Pb}/^{206}\text{Pb}$	% 1 σ	$^{207}\text{Pb}/^{238}\text{U}$	% 1 σ	$^{207}\text{Pb}/^{235}\text{U}$	$\pm 1\sigma$	$^{207}\text{Pb}/^{206}\text{Pb}$	$\pm 1\sigma$	202	204	206	207	208	232	235	238			
6	0.28127	0.01061	0.04327	0.00084	0.51	0.04796	0.00172	251.7	8.4	273.1	5.2	96.1	83.7	30	0	78.38	381	850	4167.9	1267	276207	174536		
7	0.28356	0.00909	0.04334	0.00079	0.57	0.04854	0.00148	253.5	7.2	274.7	4.9	125.7	70.4	0	0	49.86	245	687	34454	809				
Quartz-feldspar-biotite schist (sample MA11-006BV)																								
1	0.01502	0.03903	0.00071	0.33	0.04866	0.00254	245.1	12.0	246.8	4.4	131.5	118.4	10	0	54.28	270	1105	62508	940					
2	0.26837	0.00877	0.04095	0.00044	0.33	0.04909	0.00153	241.4	7.0	258.7	2.7	151.9	71.5	72	0	53.11	266	900	46700	944	197212			
3	0.29940	0.00637	0.04370	0.00034	0.35	0.04979	0.00102	265.9	5.1	185.1	47.0	0	0	10653	816	3773	193569	2596	558601					
4	0.27581	0.00996	0.04346	0.00049	0.31	0.04855	0.00167	247.3	3.1	274.3	3.1	127.6	79.2	0	0	47.41	235	709	32801	812	165891			
5	0.29195	0.00965	0.04187	0.00047	0.34	0.05138	0.00161	260.1	7.6	264.4	2.9	257.7	70.2	29	0	68.07	336	1568	74748	1165	247295			
6	0.26983	0.01171	0.04185	0.00059	0.32	0.04776	0.00197	242.6	9.4	264.3	3.7	86.2	96.0	0	16	59.66	290	1128	57105	1027	216958			
7	0.26631	0.02535	0.04179	0.00098	0.25	0.04461	0.00144	239.7	20.3	263.9	6.0	0.1	135.3	10	1	1174	53	146	6759	191	42770			
8	0.28989	0.00957	0.04241	0.00047	0.34	0.04947	0.00154	258.5	7.5	267.7	2.9	170.0	71.0	0	30	92.14	464	1231	131357	1530	330769			
9	0.27844	0.01648	0.03946	0.00072	0.31	0.05054	0.00287	249.4	13.1	289.5	4.5	220.0	126.2	0	9	27.08	139	592	32543	478	104528			
10	0.29632	0.01099	0.04209	0.00051	0.33	0.05297	0.00187	263.5	8.6	265.8	3.2	327.3	78.2	40	0	42.20	227	775	40736	734	152722			
11	0.27940	0.01856	0.04055	0.00073	0.27	0.05321	0.00173	250.2	4.5	256.3	4.5	337.8	139.8	0	15	151.14	81	268	15229	280	56894			
12	0.27109	0.01013	0.04071	0.00048	0.32	0.04867	0.00173	243.6	8.1	257.2	3.0	132.1	81.7	0	0	43.95	217	651	30191	768	164360			
13	0.27030	0.01532	0.03812	0.00075	0.35	0.05249	0.00284	242.9	12.3	241.2	4.7	307.0	118.4	53	0	53.29	284	861	41672	1007	213132			
14	0.30912	0.01071	0.03938	0.00045	0.33	0.05406	0.00178	273.5	8.3	249.0	2.8	373.5	72.1	10	0	42.98	235	847	40381	731	166449			
15	0.29082	0.00810	0.04144	0.00039	0.34	0.05104	0.00134	259.2	6.4	261.8	2.4	242.7	59.4	31	20	76.98	398	1354	7808	1315	283362			
16	0.31232	0.03378	0.04052	0.00127	0.27	0.05512	0.00164	276.0	27.7	256.1	7.9	416.8	231.6	6	2	79.1	44	123	7043	135	29792			
17	0.30215	0.02702	0.03992	0.00119	0.33	0.05659	0.00195	268.1	21.1	232.4	7.4	474.8	179.8	16	0	168.7	96	171	10462	307	64522			
18	0.29176	0.00974	0.03816	0.00044	0.35	0.05261	0.00166	259.9	7.7	241.4	2.7	312.1	70.0	41	19	83.25	443	1254	60535	1462	333064			
Quartz-feldspar-biotite schist (sample MA11-006BV)																								
1	0.02112	0.23937	0.04087	0.00079	0.27	0.04900	0.00340	261.7	16.6	258.3	4.9	147.9	155.2	46	22	139.4	70	86	4280	225	51587			
2	0.35778	0.08776	0.04096	0.00295	0.31	0.06069	0.01352	323.9	64.8	258.8	18.3	628.2	418.9	31	0	634	39	18	1260	99	23428			
3	0.21466	0.04316	0.04390	0.00219	0.25	0.04152	0.00150	209.4	0.94	276.9	13.5	0.1	180.6	0	11	103.9	44	87	2468	195	33823			
4	0.30923	0.02692	0.04154	0.00062	0.29	0.04785	0.00243	247.3	11.6	258.3	3.9	90.9	117.1	0	8	24.28	120	142	4879	409	898775			
5	0.27573	0.01454	0.04088	0.00062	0.29	0.04914	0.00149	273.6	36.1	29.0	13.9	300.4	13.9	0.1	0.0	67	32	33	1939	137	29422			
6	0.22786	0.05184	0.04770	0.00225	0.21	0.03468	0.00070	208.4	42.9	302.8	24.9	309.4	11.9	511.8	299.6	0	0	1148	68	30	1338	72	45096	
7	0.27361	0.04224	0.04224	0.00192	0.32	0.05754	0.00862	245.6	17.8	243.8	11.5	55.0	407.8	135.9	0	5	187.7	106	173	5424	337	65816		
8	0.29634	0.01954	0.04320	0.00089	0.31	0.05489	0.00348	263.5	15.3	272.6	20.9	465.1	159.0	0	17	29.70	172	232	5836	588	116121			
9	0.27598	0.02158	0.03874	0.00106	0.35	0.05634	0.00423	247.5	17.2	245.0	6.6	516.1	130.5	23.0	23	807	40	61	4437	169	335507			
10	0.22468	0.05914	0.03649	0.00257	0.27	0.04864	0.01257	205.8	49.0	231.0	16.0	124.2	12.4	0.1	0.0	905	28	60	1568	167	34402			
11	0.16223	0.04266	0.03620	0.00200	0.19	0.03089	0.00802	152.6	37.3	252.1	29.2	100.6	103.6	0	0	0	0	28	1326	72	13726			
12	0.22684	0.11559	0.04984	0.00485	0.22	0.04176	0.02057	207.6	94.0	282.8	29.9	0.1	685.5	0	31	406	17	0	1138	72	61816			
13	0.28429	0.02248	0.04037	0.00096	0.30	0.04928	0.00374	254.1	17.8	255.1	5.9	161.0	168.4	0	0	164.6	83	89	3255	277	41150			
14	0.31003	0.04637	0.04282	0.00206	0.32	0.05533	0.00794	274.2	35.9	270.3	12.7	433.2	290.6	49	22	116.2	66	45	3492	202	41150			
15	0.34142	0.03704	0.03751	0.00152	0.37	0.07186	0.00746	298.3	28.0	257.4	9.4	981.8	198.6	60	0	1561	115	104	6742	319	63137			
16	0.26982	0.02803	0.03911	0.00109	0.27	0.04637	0.00466	242.6	22.4	247.3	6.8	225.5	42.2	3	3	134.4	63	52	3585	224	52148			
17	0.28383	0.02723	0.04190	0.00125	0.31	0.05187	0.00458	253.7	21.5	264.6	7.8	279.9	197.6	0	19	153.8	81	83	4189	273	55749			
18	0.23190	0.04571	0.04261	0.00181	0.22	0.03718	0.00716	211.8	37.7	269.0	11.2	0.1	100.1	0	0	0	0	33	1843	136	31120			
19	0.23504	0.05041	0.04050	0.00196	0.27	0.05263	0.00905	254.6	39.8	255.9	12.2	312.9	350.3	0	0	0	0	778	42	47	2667	139	29202	
PLUTONIC ROCKS																								
Dawson Range batholith (sample 034239)																								
1	0.10313	0.00219	0.01564	0.00012	0.36	0.04754	0.00101	99.7	2.0	100.0	0.8	75.6	50.5	13	0	11060	552	1631	67944	2216	340250			
2	0.10592	0.00196	0.01577	0.00011	0.38	0.04813	0.00089	102.2	1.8	100.9	0.7	105.5	43.2	19	19	9601	406	621	52022	3417	525794			
3	0.10620	0.00179	0.01567	0.00010	0.38	0.04850	0.00082	102.5	1.7	100.3	0.6	123.5	39.3	14	2	15138	724	1629	129999	5929	917171			
4	0.10254	0.00186	0.01558	0.00010	0.35	0.04795	0.00087	99.1	1.7	99.7	0.7	95.8	43.6	1	6	1681	563	1461	116562	4559	712199			
5	0.10218	0.0015																						

APPENDIX 1 (continued): LA-ICP-MS data for U-Pb analysis of zircons

Fraction	Isotopic Ratios										Background corrected mean counts per second at specified mass													
	$^{20}Pb/^{234}U$	% 1 σ	$^{20}Pb/^{230}U$	% 1 σ	$^{20}Pb/^{206}Pb$	% 1 σ	$^{20}Pb/^{231}U$	% 1 σ	$^{20}Pb/^{207}Pb$	% 1 σ	$^{20}Pb/^{206}Pb$	% 1 σ	$\pm 1\sigma$	$^{20}Pb/^{207}Pb$	$\pm 1\sigma$	$^{20}Pb/^{208}Pb$	$\pm 1\sigma$	$^{20}Pb/^{206}Pb$	$\pm 1\sigma$					
17	0.10504	0.009297	0.01566	0.000016	0.36	0.04923	0.00140	101.4	2.7	100.1	1.0	158.9	65.2	11	0	13914	653	1554	120726	5480				
18	0.10520	0.009199	0.01571	0.000010	0.34	0.04973	0.000990	101.6	1.8	100.5	0.7	90.8	45.0	35	0	91.97	449	945	79945	3730				
19	0.10363	0.009213	0.01551	0.000011	0.35	0.04764	0.000986	100.1	2.0	99.2	0.7	80.4	48.7	26	1	101.41	482	1312	10430	560775				
20	0.10300	0.009188	0.01568	0.000010	0.35	0.04738	0.00086	99.5	1.7	100.3	0.7	67.6	43.2	0	19	94.39	446	839	73189	3756				
Dawson Range batholith (sample YGR-BV-004)										104.3	2.5	102.6	0.9	131.9	58.3	47	33	5045	255	828	33112	989		
1	0.10816	0.00271	0.01604	0.000015	0.37	0.04867	0.00123	101.4	1.4	102.2	0.6	105.2	33.6	0	4	104.64	494	1110	90678	4011				
2	0.10517	0.00180	0.01600	0.000010	0.37	0.04730	0.00081	101.5	1.7	102.3	0.6	63.6	41.0	28	0	117.30	571	922	75877	4498				
3	0.10500	0.00150	0.01599	0.00009	0.39	0.04812	0.00069	101.4	1.4	102.2	0.6	105.2	33.6	0	4	104.64	494	1110	90678	4011				
4	0.10548	0.00186	0.01596	0.000010	0.36	0.04816	0.00085	101.8	1.7	102.1	0.7	107.4	41.4	0	19	285.40	1373	3844	313351	11151				
5	0.10702	0.00266	0.01598	0.000015	0.38	0.04885	0.00123	103.2	2.4	102.2	0.9	140.6	57.9	53	6	97.17	468	1049	90530	3784				
6	0.10960	0.00406	0.01585	0.000022	0.37	0.04979	0.00186	105.6	3.7	101.4	1.4	185.3	84.8	60	15	107.36	2690	320.20	5852	909921				
7	0.11055	0.00212	0.01596	0.000011	0.36	0.04995	0.00097	106.5	1.9	102.1	0.7	192.8	44.4	42	0	110.70	551	1108	80469	4291				
8	0.10164	0.00196	0.01555	0.000011	0.37	0.04757	0.00092	98.3	1.8	99.5	0.7	77.2	46.2	70	0	101.03	504	859	69958	3896				
9	0.10529	0.00267	0.01602	0.000015	0.37	0.04724	0.00120	101.7	2.5	102.4	0.9	60.7	60.1	9	26	981.84	466	81519	3920	606866				
10	0.10671	0.00785	0.01605	0.000042	0.36	0.04770	0.00354	102.9	7.2	102.6	2.7	83.3	167.9	9	1	82.61	390	802	61252	3164				
11	0.10708	0.00830	0.01604	0.000020	0.35	0.04677	0.00167	103.3	3.5	102.6	1.3	37.1	83.5	0	0	204.32	1592	902	28842	3501				
12	0.10611	0.00228	0.01605	0.000012	0.35	0.04811	0.00104	102.4	2.1	102.6	0.8	104.6	50.3	7	0	106.72	498	106.7	86233	3982				
13	0.10998	0.00372	0.01575	0.000019	0.32	0.04671	0.00177	96.0	3.4	100.7	1.2	34.1	88.3	37	2	63.85	316	610	49382	2551				
14	0.10404	0.01992	0.01596	0.000011	0.37	0.04772	0.00089	100.5	1.8	102.0	0.7	84.5	44.4	28	3	78.45	366	528	42081	3157				
15	0.11022	0.00230	0.01581	0.000012	0.36	0.05038	0.00106	106.2	2.1	101.1	0.8	212.5	47.9	0	19	194.44	569	769	63080	4683				
16	0.10769	0.00255	0.01590	0.000014	0.37	0.04775	0.00114	103.8	2.3	101.7	0.9	86.0	56.5	17	22	314.49	942	942	23387	3624				
17	0.10842	0.00257	0.01607	0.000013	0.34	0.04847	0.00116	104.5	2.4	102.8	0.8	122.1	55.3	16	24	76.30	363	637	50478	2894				
18	0.10944	0.00210	0.01608	0.000011	0.36	0.04956	0.00096	105.5	1.9	102.8	0.7	174.5	44.3	0	0	57.90	280	579	48329	2214				
19	0.11449	0.00316	0.01604	0.000016	0.36	0.05032	0.00140	110.1	2.9	102.6	1.0	209.8	63.2	65	12	1356.0	670	588	48007	5255				
20	0.09905	0.00182	0.01525	0.000010	0.36	0.04724	0.00087	95.9	1.7	97.6	0.7	60.7	43.9	0	14	66.80	335	754	61826	2513				
Dawson Range batholith (sample YGR-BV-106-[b])										104.1	6.0	107.3	2.0	8.3	140.8	73	11	267.9	124	271	27505	1336		
1	0.10799	0.00650	0.01679	0.000031	0.31	0.04620	0.00282	104.1	6.0	100.5	1.1	259.7	69.2	140	11	7967	412	103.2	115385	4255				
2	0.11228	0.00339	0.01571	0.000017	0.36	0.05142	0.00158	108.0	3.1	100.5	1.0	114.3	63.8	90	14	57.66	280	639	77492	3020				
3	0.10761	0.00293	0.01619	0.000015	0.34	0.04831	0.00133	103.3	2.7	103.5	1.0	101.5	9.9	125.5	56.2	135	25	714.6	349	1324	158411	3817		
4	0.10607	0.00254	0.01587	0.000013	0.34	0.04854	0.00118	102.4	2.3	103.2	1.3	103.2	0.1	0.0	58	43.03	189	573	66206	2268				
5	0.09674	0.00415	0.01614	0.00021	0.30	0.04363	0.00190	93.8	3.8	106.5	1.0	111.5	65.1	57	7	54.08	262	664	7070	2736				
6	0.11060	0.00307	0.01613	0.000015	0.33	0.04625	0.00136	106.5	2.8	105.1	1.0	102.5	1.3	77.5	88.1	92	0	417.9	200	536	66458	2236		
7	0.10403	0.00387	0.01603	0.000020	0.34	0.04758	0.00180	100.5	3.6	102.5	1.3	105.2	3.4	99.6	1.2	156.2	83.2	120	0	437.9	217	757	839.15	2423
8	0.10402	0.00373	0.01557	0.000018	0.32	0.04918	0.00179	100.5	3.4	102.6	1.2	102.4	0.6	102.4	1.4	64.6	53.01	8	53.01	256	755	85.06	2808	
9	0.10636	0.00293	0.01568	0.000013	0.34	0.04688	0.00134	104.6	2.7	101.5	1.0	103.3	64.6	53	8	53.01	256	755	85.06	2808				
10	0.11290	0.00513	0.01595	0.000024	0.33	0.04981	0.00230	108.4	4.7	102.0	1.5	186.0	104.1	71	31	38.88	195	488	57385	2011				
11	0.11096	0.00635	0.01667	0.000029	0.30	0.04664	0.00283	106.4	5.8	106.6	1.9	130.3	131.3	1	12	21.34	104	220	24960	1097				
12	0.10729	0.00554	0.01664	0.000018	0.33	0.04719	0.00158	103.5	3.3	106.4	1.2	106.4	65.6	78.4	46	1	418.4	199	592	61085	2160			
13	0.10729	0.00226	0.01605	0.000012	0.35	0.04606	0.00102	103.4	2.1	102.6	0.6	102.4	49.4	0	28	93.42	452	235.5	243214	4923				
14	0.09973	0.00472	0.01614	0.000022	0.29	0.04616	0.00211	96.5	4.4	103.2	1.4	51.3	97.6	22	0	33.55	168	463	53385	1892				
15	0.10397	0.00431	0.01581	0.000020	0.31	0.04705	0.00198	100.4	4.0	101.1	1.3	102.4	76.6	89.4	0	0	5609	271	1092	10851	2652			
16	0.10139	0.00305	0.01588	0.000016	0.33	0.04648	0.00142	98.1	2.8	101.6	1.0	22.4	70.6	98	21	54.10	253	763	77001	2568				
17	0.10432	0.00328	0.01594	0.000017	0.34	0.04823	0.00154	100.8	3.0	101.9	1.1	110.5	73.6	111	0	57.98	282	97.8	116648	3139				
18	0.10548	0.00368	0.01579	0.000018	0.33	0.04804	0.00170	101.8	3.4	101.0	1.1	101.0	81.6	81	0	39.05	189	459	46933	2097				
19	0.10001	0.00375	0.01567	0.000020	0.34	0.04799	0.00163	96.8	3.5	100.2	1.3	97.4	89.1	41	8	49.15	237	47.9	53383	2762				
20	0.11211	0.00850	0.01684	0.00043	0.34	0.04811	0.00371	107.9	7.8	107.6	2.7	104.6	172.9	123	12	324.1	157	379	40863	1641				
Coffee Creek granite (sample YGR-BV-002)										99.2	2.6	99.8	1.0	606	64.8	13	0	5609	271	1092	10851	2652		
1	0.10266	0.00283	0.01560	0.000015	0.35	0.04723	0.00130	100.4	2.9	99.5	1.1	130.1	69.9	7	3	53.18	264	43.15	1773	907				
2	0.10351	0.00314	0.01555	0.000017	0.36	0.04863	0.00148	100.0	2.9	99.9	1.2	32.4	83.5	0	0	34.15	162	43.15	1773	907				
3	0.10254	0.00365	0.01562	0.000019	0.34	0.04667	0.00167	99.1	3.4	101.9	1.0	195.8	57.7	1	6	177.73	907	27.64	409591	8271				
4	0.110181	0.00388	0.01540	0.000021	0.36	0.04756	0.00182	98.4	3.6	98.5	1.3	102.4	76.6	89.4	0	0	51.55	250	920	82488	2477			
5	0.10181	0.00338	0.01555	0.000016	0.33	0.04648	0.00142	98.1	2.8	101.6	1.0	190.5	144.7	33	19	54.10	253	763	77001	2568				
6	0.10176	0.00651	0.01461	0.000034	0.36	0.04990	0.00325	98.4	6.0	185.3	1.4	101.4	113.0	0	0	14.47	33	19.38	200	88.8				
7	0.10201	0.00320	0.01519	0.000017	0.36	0.04823	0.00152	98.6	3.0	101.														

APPENDIX 1 (continued): LA-ICP-MS data for U-Pb analysis of zircons

Fraction	Isotopic Ratios						Isotopic Ages						Background corrected mean counts per second at specified mass											
	$^{207}\text{Pb}/^{235}\text{U}$	% 1 σ	$^{206}\text{Pb}/^{238}\text{U}$	% 1 σ	Rb	$^{207}\text{Pb}/^{206}\text{Pb}$	% 1 σ	$^{207}\text{Pb}/^{235}\text{U}$	% 1 σ	$^{207}\text{Pb}/^{238}\text{U}$	% 1 σ	$\pm 1\sigma$	$^{207}\text{Pb}/^{206}\text{Pb}$	$\pm 1\sigma$	$\pm 1\sigma$	$^{206}\text{Pb}/^{238}\text{U}$	$\pm 1\sigma$	$^{207}\text{Pb}/^{206}\text{Pb}$	$\pm 1\sigma$	$^{206}\text{Pb}/^{238}\text{U}$	$\pm 1\sigma$			
13	0.10266	0.00335	0.01556	0.00027	0.33	0.04777	0.00251	99.2	4.9	99.5	1.7	86.9	121.1	0	0	18.77	90	222	24641	901	135331	186288		
14	0.10448	0.00229	0.01566	0.00027	0.34	0.04837	0.00247	100.9	4.9	100.2	1.8	117.5	116.2	0	0	26.00	127	437	42164	1242	637230			
15	0.10965	0.00332	0.01541	0.00017	0.36	0.04518	0.00155	105.6	3.0	98.6	1.1	266.9	67.5	0	0	87.53	4.56	1268	119562	4250	522001			
16	0.10322	0.00458	0.01583	0.00025	0.36	0.04664	0.00208	99.7	4.2	101.2	1.6	30.7	103.6	0	15	77.82	1603	142208	3631	145440				
17	0.10932	0.00805	0.01669	0.00042	0.34	0.04707	0.00350	105.3	7.4	106.7	2.7	52.6	168.7	0	13	23.55	111	322	30476	1048	158469			
18	0.10110	0.00380	0.01521	0.00020	0.35	0.04749	0.00178	97.8	3.5	97.3	1.3	73.1	87.5	0	5	48.80	233	737	60813	2368	360274			
19	0.10261	0.00326	0.01576	0.00018	0.36	0.04728	0.00149	99.2	3.0	100.8	1.1	62.9	73.7	30	0	74.50	354	1101	9325	3548	530908			
20	0.10476	0.00421	0.01544	0.00022	0.35	0.04799	0.00193	101.2	3.9	98.8	1.4	97.5	93.7	0	1	10.566	509	3.189	294478	5004	769069			
Coffee Creek granite (sample 93NM-105)																								
1	0.10339	0.00220	0.01534	0.00017	0.36	0.04825	0.00143	99.9	3.0	98.1	1.1	111.5	68.4	0	16	117.31	580	1990	189507	6334	877776			
2	0.10474	0.00312	0.01561	0.00017	0.37	0.04869	0.00138	101.1	2.9	99.8	1.1	132.9	65.2	0	18	20315	1013	3402	333738	10921	1493286			
3	0.10824	0.00361	0.01599	0.00020	0.38	0.04963	0.00160	104.4	3.3	102.3	1.2	177.9	73.3	0	6	99.17	504	2341	221170	5256	711046			
4	0.24398	0.00746	0.03458	0.00039	0.37	0.05149	0.00148	221.7	6.1	219.2	2.4	263.0	64.5	10	20	291.89	1538	3079	159988	7117	967439			
5	0.10150	0.00486	0.01481	0.00025	0.35	0.04846	0.00231	98.2	4.5	94.8	1.6	121.7	108.4	0	0	40.271	2151	564	542771	2151	301957			
6	0.10009	0.00394	0.01512	0.00027	0.36	0.04837	0.00238	96.9	4.6	96.8	1.7	117.6	112.0	0	0	39.19	193	466	45604	2183	296340			
7	0.10281	0.00351	0.01514	0.00019	0.37	0.04824	0.00158	99.4	3.2	96.8	1.2	111.0	75.7	31	0	72.73	358	1100	109392	3952	549627			
8	0.10453	0.00407	0.01566	0.00022	0.36	0.04954	0.00188	101.0	3.8	100.1	1.4	173.3	86.5	0	0	36.63	286	1160	106371	3091	413592			
9	0.10374	0.00325	0.01577	0.00018	0.36	0.04777	0.00141	100.2	3.0	100.9	1.1	86.8	69.7	0	13	20375	992	47.07	441060	10790	1474918			
10	0.10281	0.00406	0.01522	0.00022	0.36	0.04854	0.00187	99.4	3.7	98.0	1.4	125.9	83.1	0	0	85.98	425	1609	159007	46667	646012			
11	0.10473	0.00366	0.01558	0.00020	0.37	0.04814	0.00161	101.1	3.4	99.6	1.3	106.3	77.4	32	20	94.24	462	2090	193303	4977	690328			
12	0.10300	0.00375	0.01585	0.00021	0.36	0.04675	0.00164	99.5	3.5	101.4	1.3	36.4	82.0	74	14	66.36	315	1111	107044	3459	477455			
13	0.10514	0.00529	0.01556	0.00028	0.36	0.04927	0.00246	101.5	4.9	99.6	1.8	160.6	112.7	62	20	3412	170	494	50443	1833	249767			
14	0.10278	0.00333	0.01529	0.00023	0.36	0.04895	0.00202	99.3	4.0	97.8	1.5	145.7	93.8	74	0	85.71	426	1615	149740	4678	638081			
15	0.10584	0.00406	0.01537	0.00021	0.36	0.04909	0.00182	102.1	3.7	98.3	1.4	151.9	84.7	26	16	86.94	433	1310	126233	4619	643845			
16	0.10492	0.0025	0.01590	0.00028	0.35	0.04809	0.00238	101.3	4.8	101.7	1.8	103.5	113.0	0	0	47.75	233	710	74355	2505	341546			
17	0.10861	0.00392	0.01521	0.00020	0.36	0.05174	0.00174	104.7	3.6	97.3	1.3	273.9	77.1	6	27	20212	1035	6714	615204	10958	1502498			
18	0.10907	0.00461	0.01528	0.00023	0.36	0.05211	0.00211	105.1	4.2	97.4	1.5	249.7	92.1	0	12	43.19	224	736	67610	2316	320953			
19	0.10310	0.00423	0.01568	0.00023	0.36	0.04662	0.00185	99.6	3.9	100.3	1.5	29.9	92.8	0	27	57.49	271	821	76380	2969	416182			
20	0.10622	0.00358	0.01585	0.00019	0.36	0.04821	0.00153	102.5	3.3	101.4	1.2	109.4	73.2	89	0	61019	2978	22748	2E+06	31613	4368048			
Coffee Creek granite (sample 93NM-107)																								
1	0.10349	0.00143	0.01561	0.00009	0.42	0.04802	0.00067	100.0	1.3	99.9	0.6	98.9	34.0	45	13	19926	969	3.667	404003	10955	1804307			
2	0.11027	0.00158	0.01609	0.00009	0.39	0.04912	0.00072	106.2	1.5	102.9	0.6	153.7	33.8	0	0	17501	871	1841	203355	9242	1537184			
3	0.10469	0.00139	0.01552	0.00009	0.44	0.04834	0.00065	101.1	1.3	99.3	0.6	115.9	31.6	10	20	27249	1339	7450	900778	15197	252653			
4	0.10338	0.00288	0.01559	0.00016	0.37	0.04798	0.00137	99.7	2.7	97.7	1.0	97.1	67.3	12	0	96.18	467	2576	282684	5296	871889			
5	0.10283	0.00146	0.01548	0.00009	0.41	0.04811	0.00069	99.4	1.3	99.1	0.6	104.9	33.7	0	21	259.62	1265	4034	451622	14426	2368088			
6	0.10297	0.00097	0.01559	0.00007	0.48	0.04778	0.00045	99.5	0.9	99.7	0.4	87.6	23.4	21	1	39500	1911	6471	703634	21778	3577980			
7	0.10589	0.00156	0.01541	0.00009	0.40	0.04897	0.00073	102.2	1.4	104.6	0.6	146.3	34.8	0	23	18733	929	2609	31356	10297	1716416			
8	0.10197	0.00140	0.01539	0.00009	0.43	0.04788	0.00067	98.6	1.3	98.4	0.6	92.3	33.8	0	12	27552	1335	6336	70124	15385	2527561			
9	0.10126	0.00409	0.01529	0.00022	0.36	0.04708	0.00194	97.9	3.8	97.8	1.4	53.1	96.0	108	0	48.16	229	834	91738	2665	44486			
10	0.10266	0.00167	0.01534	0.00010	0.40	0.04808	0.00080	99.2	1.5	98.1	0.6	103.2	38.8	42	44	20654	1005	3880	47.386	11518	1899842			
11	0.10328	0.00146	0.01547	0.00009	0.41	0.04807	0.00056	99.8	1.3	98.9	0.6	102.8	33.6	43	0	22282	1081	2748	308437	12325	2026927			
12	0.10122	0.00108	0.01547	0.00007	0.42	0.04706	0.00051	97.9	1.0	98.9	0.5	51.9	25.0	0	2	29.94	1404	4534	53.2727	16343	268994			
13	0.10438	0.00210	0.01548	0.00012	0.39	0.04815	0.00099	100.8	1.9	99.0	0.8	106.9	47.8	32	0	99.46	484	2369	257586	5454	905511			
14	0.11169	0.00206	0.01528	0.00011	0.39	0.04717	0.00098	107.5	1.9	97.8	0.7	272.4	42.7	57	55	12.413	13647	2278058						
15	0.10378	0.00144	0.01549	0.00009	0.42	0.04793	0.00061	100.3	1.3	99.1	0.6	94.6	34.1	16	10	9880	1448	4300	48201	16476	2717852			
16	0.10438	0.00118	0.01533	0.00008	0.46	0.04857	0.00036	100.8	1.1	98.1	0.5	12												

APPENDIX 1 (continued): LA-ICP-MS data for U-Pb analysis of zircons

Fraction	Isotopic Ratios						Isotopic Ages						Background corrected mean counts per second at specified mass										
	$^{207}\text{Pb}/^{235}\text{U}$	% 1 σ	$^{208}\text{Pb}/^{232}\text{U}$	% 1 σ	ρho	$^{207}\text{Pb}/^{206}\text{Pb}$	% 1 σ	$^{207}\text{Pb}/^{238}\text{U}$	% 1 σ	$\pm 1\sigma$	$^{206}\text{Pb}/^{207}\text{Pb}$	$\pm 1\sigma$	$\pm 1\sigma$	202	204	206	207	208	232	235	238		
8	0.05539	0.00704	0.00899	0.00030	0.26	0.04413	0.00570	54.7	6.8	57.7	1.9	0.1	187.3	0	0	966	42	191	47.019	716	158022		
9	0.05015	0.01224	0.00905	0.00040	0.18	0.03881	0.00955	49.7	11.8	58.1	2.6	0.1	117.1	23	0	493	19	101	2163.5	355	80214		
10	0.04233	0.01804	0.00865	0.00051	0.14	0.03604	0.01545	42.1	17.6	55.5	3.3	0.1	263.1	41	41	233	9	51	15566	201	43204		
11	0.05107	0.00825	0.00916	0.00032	0.22	0.03957	0.00646	50.6	8.0	58.8	2.0	0.1	648	25	120	28156	469	104654					
12	0.08295	0.03003	0.00850	0.00072	0.23	0.06746	0.02486	80.9	28.2	54.6	4.6	0.0	40	8	188	12	54	10182	143	32829			
13	0.05907	0.00569	0.00875	0.00027	0.32	0.04902	0.00483	58.3	5.5	56.1	1.7	1.7	216.0	61	3	1224	60	173	36942	950	207605		
14	0.06656	0.01159	0.00844	0.00039	0.27	0.05989	0.01064	65.4	11.0	54.2	2.5	2.5	344.2	18	2	399	23	61	17326	336	70346		
15	0.06503	0.00747	0.00895	0.00033	0.32	0.05622	0.00663	64.0	7.1	57.4	2.1	460.2	242.9	0	13	763	43	103	21803	618	126965		
16	0.05293	0.00944	0.00945	0.00045	0.27	0.04176	0.00758	52.4	9.1	60.6	2.9	0.1	163.7	44	16	1003	42	170	41699	743	158430		
17	0.05040	0.00656	0.00856	0.00027	0.24	0.04180	0.00552	49.9	6.4	54.9	1.8	0.1	64.9	0	0	855	35	67	19465	666	149306		
18	0.06156	0.00602	0.00910	0.00023	0.26	0.04869	0.00483	60.7	5.8	58.4	1.5	1.5	133.0	217.8	0	0	957	46	131	29664	712	157333	
19	0.03562	0.01216	0.00817	0.00038	0.14	0.03320	0.01071	35.5	11.9	52.4	2.5	0.1	0.0	0	0	433	13	118	21499	357	79560		
20	0.06905	0.00647	0.00908	0.00028	0.33	0.05667	0.00544	67.8	6.2	58.3	1.8	477.9	200.1	4	20	882	50	230	43210	682	145736		